Scientific Reports

https://doi.org/10.1038/s41598-025-34626-8

Article in Press

# Comprehensive proteomics analysis of bovine sperm head plasma membrane associated with fertility

Received: 30 June 2025

Accepted: 30 December 2025

Published online: 03 April 2026

Cite this article as: Imran M., Buhr M.M., Chumala P. *et al.* Comprehensive proteomics analysis of bovine sperm head plasma membrane associated with fertility. *Sci Rep* (2025). https://doi.org/10.1038/s41598-025-34626-8

Muhammad Imran, Mary M. Buhr, Paulos Chumala & George S. Katselis

# Comprehensive Proteomics Analysis of Bovine Sperm Head Plasma Membrane Associated with Fertility

**Muhammad Imran[1,2,3], Mary M. Buhr[1], Paulos Chumala[2], George S. Katselis[2,4,*]**

1-Department of Animal and Poultry Science, University of Saskatchewan, Saskatoon, SK, Canada

2-Canadian Centre for Rural and Agricultural Health, University of Saskatchewan, Saskatoon, SK, Canada

3-Women and Children's Health Research Institute, and Department of Obstetrics & Gynecology, Faculty of Medicine and Dentistry, and The Metabolomics Innovation Centre, University of Alberta, Edmonton, AB, Canada (Present Address)

4-Department of Medicine, College of Medicine, University of Saskatchewan, Saskatoon, SK, Canada

***Correspondence to George S. Katselis:** george.katselis@usask.ca, Department of Medicine, College of Medicine, and Canadian Centre for Rural and Agricultural Health, University of Saskatchewan, 104 Clinic Place (Room 1246, Health Sciences E-Wing) Saskatoon, SK, S7N 2Z4, Canada



## Abstract

Bull fertility impacts herd fertility, but accurately predicting male fertility from sperm characteristics is difficult once extremes are removed. The objectives of this study were identification, relative quantification, and comparison of sperm head plasma membrane (HPM) proteomics in bulls of differing bull fertility index (BFI). HPM from one fresh ejaculate from 16 Holstein bulls (8 each high and low fertility) was extracted, digested and assessed by liquid chromatography-tandem mass spectrometry (LC-MS/MS). The MS spectra were aligned to UniProtKB mammals, identified, and characterized by Spectrum Mill. Mass Profiler Professional statistical analysis of the 22,117 total proteins identified in all bulls, after database search, revealed 67 proteins [unique plus homologous, 1% false discovery rate] whose abundance differed at least 2-fold (differentially abundant proteins, DAPs) between

the 3 bulls each with highest and lowest BFI [high fertility (HF) BFI 105.66 ± 0.54 >low fertility (LF) BFI 91.33 ± 1.44; $p<0.01$]. Gene ontology assigned the 48 DAPS increased in HF to sperm-specific function and fertility-related mechanisms, and the 19 HF-decreased DAPs primarily to catalytic and transporter activity. Meta analysis and linear regression each confirmed that the BFI of the 6 HF/LF bulls significantly correlated to the DAPS (regression $r^2=0.65$ to 0.97, $p\leq0.05$), but importantly in the 16-bull population, linear regression found that 38 of the HF-increased DAPS positively correlated to BFI ($r^2=0.29$ to 0.66; $p\leq0.05$), and 4 of the HF-decreased DAPS negatively correlated ($r^2=0.26$ to 0.44; $p\leq0.05$). In summary, this study identified HPM proteins with important roles in sperm fertilization and significant correlations with bull fertility.

**Key words**: Fertilization, Predicting Bull Fertility, Sperm HPM, Fertility Biomarkers, Mass Spectrometry-based Proteomics



## Introduction

Reproductive efficiency of the male includes the ability of sperm to fertilize oocytes [1] which necessitates motility, functional mitochondria, DNA decondensation, and an active and intact sperm plasma membrane [2], so sperm can reach, recognize, bind to and fuse with the oocyte. All these events are essential for successful fertilization and any defect can cause sub-fertility or infertility [1].

More than 70% of dairy cows are bred by artificial insemination (AI) using frozen semen from genetically superior bulls, but only 50% of inseminations result in successful pregnancies. One accepted measure of dairy bull fertility is the percentage of cows not returning to estrus after insemination (non-return rate, NRR), after

adjustment for various management factors (e.g., age of cow, number of parities, herd, etc.), and other variables [3]. Bull fertility Index (BFI) is calculated from the adjusted NRR from thousands of inseminations per bull and hundreds of bulls contribute to the population average BFI of 100 [4, 5]. Diagnosing bull fertility is essential in the breeding industry to optimize male fertility and reduce pregnancy failures [6]. Since assessing bull fertility by natural mating or AI is time consuming, expensive and retrospective, a laboratory test of raw semen that efficiently economically and reliably predicted fertility would be highly valuable. Current methods include sperm structural and functional parameters such as sperm kinetic parameters by CASA, sperm oocyte penetration assay, semen biochemical compounds, acrosome and plasma membrane integrity, mitochondrial membrane potential, and sperm DNA fragmentation [7] However, none of these is sufficiently accurate and repeatable in predicting *in vivo* bull fertility [7, 8].

Omics approaches, including proteomics, may hold the key for accurate diagnosis of male infertility [9]. Various proteomics studies have been performed to identify protein biomarkers in whole bull sperm associated with fertility by comparing whole sperm from high versus low fertility bulls in buffalo [10], cattle [4] and boar [11]. Studies to characterize the semen proteome have also been done in frozen bull semen [12], in *Bos taurus* seminal plasma [7, 13], fresh [7] and frozen whole sperm [14, 15] and sperm surface proteins [16]. These studies have, however, been limited by the smaller number of inseminations from bulls evaluated, and they lack in-depth analysis of sperm head plasma membrane (HPM) and prediction of complex interactions among HPM proteins, which control sperm-oocyte binding and fertilization.

The plasma membrane of bull sperm has significant roles in progressive motility, fertilization, and transport of various ions across the membrane [17]. Capacitation of sperm in the female tract, a crucial process initiating actual fertilization, involves remodeling of the plasma membrane, predominantly the HPM, that primes sperm for acrosomal exocytosis (AE), binding to oocyte [17] and various important physiological functions during fertilization [18]. The precise trigger for capacitation is not yet known.

The importance of the HPM in capacitation, AE, and sperm-oocyte interactions is well established [17, 18], but the HPM's specific protein composition is unknown. Therefore, identification of a cohort of structural and functional sperm HPM proteins impacting the mechanism of fertilization would be unique, important, and necessary. The specific objectives of this proteomics analysis were the identification and relative quantification of proteins in sperm HPM from bulls of differing fertility, the elucidation of protein-protein interactions and extrapolating their cellular functions and biological pathways impacting bull fertility.



## Results

The motility of the sperm from the two groups of bulls did not differ on collection at the facility (79±1% for each group, n=8 per group) or as measured by CASA at our laboratory (32.3±4.8 = 34.9±3.9% motile, HF=LF, $p>0.05$).

### Protein Identification and Complete Interactome of HPM

The combined unique and common sperm HPM proteins from all 16 bulls totalled 22,117 after database search. The 3 bulls with the lowest fertility bulls (LF; BFIs 88-94) bulls had 4,040 total identified proteins (1,199 unique) and three bulls with the highest fertility (HF; BFIs 105-107) had 4,074 (1,156 unique), respectively. Of the 22,117 bovine sperm HPM total proteins in all bulls, 4,273 could be annotated and

Cytoscape software constructed a complete interactome (Fig 1) whose complexity and connectivity manifested in 4,273 nodes (each an identified HPM protein annotated to mammals) and 27,473 edges (each indicating interaction).

Mass Profiler Professional (MPP) analysis compared the intensities of the annotated proteins in LF and HF, finding 67 proteins whose spectral intensities differed by at least 2-fold [differentially abundant proteins (DAPs); $p<0.05$; false discovery rate (FDR) at <1%]. Interestingly, all down-regulated DAPs occurred in one of the two major clusters found in the interactome (Fig 1). The relationship of the 67 DAPs to BFI of the animals was confirmed by meta-analysis, as indicated in the heat map (Fig 2), where the 67 DAPs demonstrated a well-defined association with the fertility group/BFI.

## Multivariate Analysis of Identified Proteins

Multivariate analysis of the DAPs identified clear fixed clustering (Fig 3, red and yellow circles) separating the two fertility groups. Principal component analysis (PCA) showed the 3-dimensional spread of the 67 DAPs differing between LF and HF bulls as did the spread of the average DAPs (Fig 3 a, b). Protein abundance, as shown by the dot size, also differed in both analyses. Heat maps were drawn for the 67 DAPs, separately representing the 48 DAPs that were increased in HF vs LF (Fig 4 a) and the 19 that were decreased in HF vs LF (Fig 4b).

## Identification of Sub-Networks with FC Proteins

Cytoscape software visualized integrated sperm regulatory sub-networks for each of the sperm HPM DAPs with non-DAPs. Representative networks selected from these illustrate the identified sperm function networks (Fig 5 a-m, HF-increased DAPs; Fig 6 a-b, HF-decreased DAPs).

## DAPs Protein-Protein Interaction and STRING Network

The STRING protein-protein interaction (PPI) network constructed on the setting "evidence based" and mapping 7 database channels, found 24 connected nodes in the 48 DAPs increased in HF with 28 edges with significant PPI enrichment ($p<0.05$; $9.21x10^{-12}$; Fig 7), representing both functional and physical protein associations. The network of the 19 DAPs decreased in HF was non-significant (PPI enrichment 0.177; $p>0.05$), indicating no significant interaction among DAP nodes.

## Identification of Key Proteins

The Molecular Complex Detection (MCODE) analysis of the HF-increased DAPs' PPI networks shown in Fig 7 detected densely connected regions based on highest k-core of the vertex neighborhood. MCODE mapped three different clusters (Fig 8, Table 1) with 12 key proteins in the HF-increased DAPs; no clusters were detected by MCODE in the DAPs decreased in HF.

**Table 1. MCODE Analysis of the DAPs increased in HF**

| Clusters | Protein Name | Accession Number | MCODE score |
|---|---|---|---|
| Cluster 1 | UQCRH | P00126 | 3.33 |
| | ATP5H | P13620 | |
| | ATP5F1 | P13619 | |
| | AK8 | Q96MA6 | |
| Cluster 2 | ROPN1L | Q3T064 | 3.33 |
| | RIBC2 | Q32LJ7 | |
| | RSPH6A | Q9H0K4 | |
| | DNAI1 | Q32KS2 | |
| Cluster 3 | AKAP3 | O77797 | 2.67 |
| | ACRBP | Q29016 | |
| | SPATA19 | Q3SZQ3 | |
| | ODF3 | Q2TBH0 | |

MCODE Score: the cluster's computed score which is defined as the product of the number of proteins (vertices) and the density in the complex subgraph (|V| x DC). The default threshold score is 0.2; values above threshold indicate that clusters are more densely connected.

## Gene Ontology Functional Analysis of DAPs (Molecular and Biological Functions)

Gene ontology (GO) analysis by PANTHER databases detected functional enrichment of molecular functions of DAPs increased or decreased in HF (Fig 9). Significantly more increased than decreased DAPs had binding functions (50.0 vs 30.8%, $p<0.05$, Fig 9 a, b), while more decreased proteins had catalytic activity than did increased proteins (61.5 vs 40.0%, $p\leq0.05$). HF-decreased DAPs uniquely included transporter activity, while HF-increased proteins uniquely included molecular function regulation. STRING databases identified GO biological processes (Table 2) which included eight biological processes in the HF-increased proteins that were highly relevant and essential for sperm development and function, and eight biological processes in the HF-decreased proteins that were relevant to catalytic enzymes and metabolic processes. The nucleoside triphosphate biosynthetic process was the one common process identified in both increased and decreased proteins.

**Table 2. Functional Enrichment Analysis from GO of DAPs Increased or Decreased (Up/Down) in HPM of High vs Low Fertility Bulls - Biological Process**

| Term ID | Up/Down | Term Description | OGC[a] | BGC[b] | Strength | FDR[c] |
|---|---|---|---|---|---|---|
| GO:0007283 | Up | spermatogenesis | 9 | 490 | 0.8 | 0.003 |
| GO:0019953 | Up | sexual reproduction | 10 | 764 | 0.7 | 0.005 |
| GO:0009142 | Up | nucleoside triphosphate biosynthetic process | 4 | 103 | 1.2 | 0.018 |
| GO:0003341 | Up | cilium movement | 3 | 61 | 1.3 | 0.043 |
| GO:0007286 | Up | spermatid development | 4 | 137 | 1.0 | 0.043 |
| GO:0009123 | Up | nucleoside monophosphate metabolic process | 5 | 262 | 0.9 | 0.043 |
| GO:0009141 | Up | nucleoside triphosphate metabolic process | 5 | 246 | 0.9 | 0.043 |
| GO:0022414 | Up | reproductive process | 11 | 1350 | 0.5 | 0.043 |
| GO:0009132 | Down | nucleoside diphosphate metabolic process | 5 | 56 | 1.9 | 2.36E-06 |
| GO:0009142 | Down | nucleoside triphosphate biosynthetic process | 5 | 103 | 1.7 | 1.07E-05 |
| GO:0009165 | Down | nucleotide biosynthetic process | 6 | 291 | 1.3 | 4.50E-05 |

| | | | | | | |
|---|---|---|---|---|---|---|
| GO:0009206 | Down | purine ribonucleoside triphosphate biosynthetic process | 4 | 86 | 1.7 | 0.001 |
| GO:0006754 | Down | ATP biosynthetic process | 3 | 39 | 1.9 | 0.006 |
| GO:0009435 | Down | NAD biosynthetic process | 3 | 51 | 1.8 | 0.009 |
| GO:0009152 | Down | purine ribonucleotide biosynthetic process | 4 | 189 | 1.3 | 0.001 |
| GO:0019674 | Down | NAD metabolic process | 3 | 66 | 1.7 | 0.001 |

a = Observed Gene Count; b = Background Gene Count; c = False Discovery Rate

## Relationship of DAPs to Fertility Measures

Linear regression first compared DAPs intensities identified with HF and LF bulls and their respective BFIs (n = 3 each) and secondly compared these same proteins taking the intensities and BFIs from the entire population of all 16 bulls. Not surprisingly, regressions of the intensities of the 48 HF-increased DAPs to their BFIs in the HF and LF bulls were significantly positive (Table 3; $r^2$=0.65 to 0.97, p≤0.05), and the regressions of the HF's and LF's 19 HF-decreased DAPs intensities to their BFIs were all significantly negative (Table 4; $r^2$=0.76 to 0.96, p≤0.02).

**Table 3. Regression Analysis of HF-increased DAPs Intensities on BFI (n = 6 & n = 16)**

| DAPs | | Linear Regression: DAP Intensity to BFI | | | |
|---|---|---|---|---|---|
| | | n = 6 | | n = 16 | |
| Accession # | Protein Name | $r^2$ | p-Value | $r^2$ | p-Value |
| **Q2T9U2** | Outer dense fiber protein 2 | 0.904 | 0.004 | 0.493 | 0.002 |
| **O77797** | A-kinase anchor protein 3 | 0.882 | 0.006 | 0.424 | 0.006 |
| **Q2TBH0** | Outer dense fiber protein 3 | 0.704 | 0.037 | 0.430 | 0.006 |
| **Q32LJ7** | RIB43A-like with coiled-coils protein 2 | 0.700 | 0.038 | 0.451 | 0.004 |
| **Q9N2J2** | Phospholipid hydroperoxide glutathione peroxidase | 0.882 | 0.005 | 0.661 | 0.001 |
| **A6QLU1** | Glycerol-3-phosphate dehydrogenase, mitochondrial | 0.885 | 0.005 | 0.554 | 0.001 |
| **Q32KS2** | Dynein intermediate chain 1, axonemal | 0.794 | 0.017 | 0.368 | 0.013 |
| **P79136** | F-actin-capping protein subunit beta | 0.836 | 0.011 | 0.468 | 0.004 |
| **P00669** | Seminal ribonuclease | 0.717 | 0.033 | 0.341 | 0.018 |

| | | | | | |
|---|---|---|---|---|---|
| **P17697** | Clusterin | 0.793 | 0.017 | 0.346 | 0.017 |
| **Q86TE4** | Leucine zipper protein 2 | 0.896 | 0.004 | 0.387 | 0.010 |
| **Q2T9T0** | Protein phosphatase 1 regulatory subunit 32 | 0.773 | 0.021 | 0.338 | 0.018 |
| **P19858** | L-lactate dehydrogenase A chain | 0.978 | <0.001 | 0.560 | 0.001 |
| **Q2T9X5** | Uncharacterized protein C7orf61 homolog | 0.759 | 0.024 | 0.230 | 0.1<p>0.05 |
| **P00727** | Cytosol aminopeptidase | 0.955 | 0.001 | 0.432 | 0.006 |
| **P35662** | Cylicin-1 | 0.652 | 0.052 | 0.294 | 0.030 |
| **Q3SZT6** | Protein Flattop | 0.712 | 0.035 | 0.491 | 0.003 |
| **Q3T064** | Ropporin-1 | 0.885 | 0.005 | 0.564 | 0.001 |
| **P13619** | ATP synthase F (0) complex subunit B1, mitochondrial | 0.793 | 0.017 | 0.432 | 0.006 |
| **Q6ZQR2** | Cilia- and flagella-associated protein 77 | 0.881 | 0.006 | 0.437 | 0.005 |
| **Q5CZC0** | Fibrous sheath-interacting protein 2 | 0.906 | 0.003 | 0.581 | 0.001 |
| **Q29016** | Acrosin-binding protein (Fragment) | 0.828 | 0.012 | 0.370 | 0.012 |
| **Q96MR6** | Cilia- and flagella-associated protein 57 | 0.654 | 0.051 | 0.537 | 0.001 |
| **P13620** | ATP synthase subunit d, mitochondrial | 0.878 | 0.006 | 0.320 | 0.022 |
| **P00126** | Cytochrome b-c1 complex subunit 6, mitochondrial | 0.775 | 0.021 | 0.283 | 0.034 |
| **Q3SZR5** | Protein FAM166C | 0.861 | 0.008 | 0.302 | 0.028 |
| **A7MBH5** | Coiled-coil domain-containing protein 151 | 0.922 | 0.002 | 0.016 | >0.1 |
| **Q0VFZ6** | Coiled-coil domain-containing protein 173 | 0.837 | 0.011 | 0.015 | >0.1 |
| **Q32P85** | Dynein light chain roadblock-type 2 | 0.889 | 0.005 | 0.287 | 0.032 |
| **Q9H0K4** | Radial spoke head protein 6 homolog A | 0.842 | 0.010 | 0.190 | 0.1<p>0.05 |
| **Q3SZQ3** | Spermatogenesis-associated protein 19, mitochondrial | 0.959 | 0.001 | 0.479 | 0.003 |
| **Q8WUD1** | Ras-related protein Rab-2B | 0.930 | 0.002 | 0.780 | <0.001 |
| **Q9Z280** | Phospholipase D1 | 0.788 | 0.018 | 0.057 | 0.1<p>0.05 |
| **O95757** | Heat shock 70 kDa protein 4L | 0.793 | 0.017 | 0.004 | >0.1 |
| **Q6P2I7** | Endogenous Bornavirus-like nucleoprotein 2 | 0.788 | 0.018 | 0.023 | >0.1 |
| **A6NG13** | Alpha-1,3-mannosyl-glycoprotein 4-beta-N-acetylglucosaminyltransferase-like protein MGAT4D | 0.781 | 0.020 | 0.029 | >0.1 |
| **O94810** | Regulator of G-protein signaling 11 | 0.914 | 0.003 | 0.323 | 0.022 |
| **P17156** | Heat shock-related 70 kDa protein 2 | 0.933 | 0.002 | 0.339 | 0.1<p>0.05 |
| **Q96MA6** | Adenylate kinase 8 | 0.934 | 0.002 | 0.326 | 0.021 |

| | | | | | |
|---|---|---|---|---|---|
| **Q9C0F0** | Putative Polycomb group protein ASXL3 | 0.924 | 0.002 | 0.556 | 0.021 |
| **Q60698** | Ski oncogene | 0.927 | 0.002 | 0.489 | 0.004 |
| **O43451** | Maltase-glucoamylase, intestinal | 0.931 | 0.002 | 0.255 | 0.055 |
| **Q63647** | Proline-rich nuclear receptor coactivator 1 | 0.933 | 0.002 | 0.343 | 0.017 |
| **E1BBQ2** | Probable G-protein coupled receptor 158 | 0.925 | 0.002 | 0.553 | 0.022 |
| **Q9P217** | Zinc finger SWIM domain-containing protein 5 | 0.871 | 0.007 | 0.531 | 0.026 |
| **P59796** | Glutathione peroxidase 6 | 0.922 | 0.002 | 0.221 | 0.1<p>0.05 |
| **P56965** | N(G),N(G)-dimethylarginine dimethylaminohydrolase 1 | 0.929 | 0.002 | 0.557 | 0.021 |
| **O08876** | Krueppel-like factor 10 | 0.929 | 0.002 | 0.353 | 0.020 |

$r^2$= r-square, BFI=Bull Fertility Indexes, Accession # = Accession number of DAPs derived from UniProt database.

**Table 4. Regression Analysis of HF-decreased DAPs Intensities on BFI (n = 6 & n = 16)**

| | **Down-Regulated DAPs** | **Linear Regression of DAPs intensities to BFI** | | | |
|---|---|---|---|---|---|
| | | n = 6 | | n = 16 | |
| Accession # | Protein Name | $r^2$ | p-Value | $r^2$ | p-Value |
| **P0CB32** | Heat shock 70 kDa protein 1-like | -0.953 | 0.001 | -0.235 | 0.1<p>0.05 |
| **Q9WV27** | Sodium/potassium-transporting ATPase subunit alpha-4 | -0.939 | 0.001 | -0.272 | 0.039 |
| **P61019** | Ras-related protein Rab-2A | -0.912 | 0.003 | -0.187 | 0.1<p>0.05 |
| **Q9XSJ4** | Alpha-enolase | -0.967 | <0.001 | -0.192 | 0.1<p>0.05 |
| **Q6B857** | Cilia- and flagella-associated protein 20 | -0.895 | 0.004 | -0.231 | 0.1<p>0.05 |
| **Q4R3W4** | Adenylate kinase 8 | -0.955 | 0.001 | -0.197 | 0.1<p>0.05 |
| **Q5JRX3** | Presequence protease, mitochondrial | -0.954 | 0.001 | -0.241 | 0.1<p>0.05 |
| **Q99MH5** | Nucleoside diphosphate kinase homolog 5 | -0.912 | 0.003 | -0.186 | 0.1<p>0.05 |
| **P00517** | cAMP-dependent protein kinase catalytic subunit alpha | -0.913 | 0.003 | -0.246 | 0.051 |
| **Q3V0E1** | Uncharacterized protein C9orf131 homolog | -0.949 | 0.001 | -0.440 | 0.007 |
| **Q7Z745** | Maestro heat-like repeat-containing protein family member 2B | -0.920 | 0.003 | -0.253 | 0.047 |
| **Q8K410** | Disintegrin and metalloproteinase domain-containing protein 32 | -0.930 | 0.002 | -0.245 | 0.051 |
| **Q5TCS8** | Adenylate kinase 9 | -0.769 | 0.022 | -0.188 | 0.1<p>0.05 |
| **Q07113** | Cation-independent mannose-6-phosphate receptor | -0.905 | 0.004 | -0.223 | 0.1<p>0.05 |

| | | | | | |
|---|---|---|---|---|---|
| **Q3ZBD7** | Glucose-6-phosphate isomerase | -0.841 | 0.010 | -0.173 | >0.1 |
| **E1BNQ4** | ATP-dependent (S)-NAD(P)H-hydrate dehydratase | -0.871 | 0.007 | -0.133 | >0.1 |
| **Q8NDM7** | Cilia- and flagella-associated protein 43 | -0.887 | 0.005 | -0.221 | 0.1<p>0.05 |
| **Q8SPU8** | Dehydrogenase/reductase SDR family member 4 | -0.931 | 0.002 | -0.067 | >0.1 |
| **Q5E9H5** | Mitochondrial chaperone BCS1 | -0.842 | 0.010 | -0.266 | 0.049 |

$r^2$ = r-square (in negative values), BFI=Bull Fertility Indexes, Accession # = Accession number of DAPs derived from UniProt database.

Of greater interest were the outcomes of regressions testing the entire 16-bull population. The intensity of the DAPs identified in each bull were regressed against the full range of the 16 BFIs. Of the 48 HF-increased DAPs, 10 were missing in 5-7 bulls with a range of BFIs and so eliminated from regression testing. The intensities of the remaining 38 HF-increased DAPs had a significantly positive relationship to BFI (Table 3, $p \leq 0.034$), and of those, 10 had an $r^2 > 0.50$ ($p \leq 0.026$). All 19 HF-decreased DAPs were detected in all 16 bulls (Table 4), of which four DAPs had significant, negative, regressions to BFI ($r^2 = 0.27$ to 0.44; $p \leq 0.05$; two decreased DAPS had linear regressions $p = 0.051$).

The sub-networks of three HF-decreased DAPs with significant ($p < 0.05$) and negative $r^2$ values, along with their PPIs detected in all 16 bulls are shown in Fig 10 a-c. The decreased DAP, sodium/potassium-transporting ATPase subunit alpha-4 (Fig 10 a) was connected to non-DAPs interacting partners sodium/potassium-transporting ATPase subunit alpha-3, sodium/potassium-transporting ATPase subunit alpha-2, potassium-transporting ATPase alpha chain 2, cilia- and flagella-associated protein 45, cAMP-dependent protein kinase catalytic subunit gamma, testis-specific serine/threonine-protein kinase 6, and phospholipid-transporting ATPase ABCA7. The cluster depicted in Fig 10b was largely comprised of mitochondrial proteins: mitochondrial chaperone BCS1 HF-increased DAP connected to the HF-decreased DAPs cytochrome b-c1 complex subunit 6, mitochondrial; and ATP synthase F (0)

complex subunit B1, mitochondrial. In non-DAPs, the majority of the proteins were multiple isoforms of cytochrome b-c1 complex and NADH dehydrogenase. In Fig 10c, the HF-decreased DAP maestro heat-like repeat-containing protein family member 2B only interacted with non-DAP hydrocephalus-inducing protein homolog.

## Discussion

Sperm HPM proteomics comparing high and low fertility Holstein bulls for the first time have provided significant new insights, first into processes in sperm fertilization and second into controllers of *in vivo* fertility. High fertility in bulls was strongly correlated with the presence of a cohort of structural and functional proteins whose abundance in sperm HPM differed significantly among bulls of differing fertility. Identified roles and molecular interactions of membrane proteins in sperm motility, sperm capacitation, AE, metabolism, signaling pathways, cytoskeletal structure and sperm oocyte recognition, and their relative abundance in high- or low-fertility bulls have expanded our understanding of protein regulation of sperm membrane mechanisms active in fertilization.



Fresh ejaculates were obtained from 16 Holstein Friesian bulls whose rigorously determined BFIs allowed them to be divided into high (BFI > 101, n = 8) and low (BFI < 101, n = 8) fertility groups. The current research's focus on the *Bos taurus* sperm HPM differed from previous proteomics studies of whole sperm [15] and/or seminal plasma [7], and allowed deep proteomics analysis on this membrane's crucial roles in capacitation and sperm-egg fusion [18].

Semi-quantitative liquid chromatography-tandem mass spectrometry (LC-MS/MS) identified 22,117 unique and homologous total proteins in all bulls aligned to the UniProt mammals database, which were rigorously validated by Spectrum Mill at both the peptide and protein level [19]. These identified HPM proteins displayed significant

interactions as they clustered in their interactome (Fig 1). Rigorous big data analytics identified 67 DAPs in these bull sperm HPM proteins that differed in abundance by at least two-fold between the HF and LF bulls (Table 2; 48 HF>LF; 19 HF<LF). These DAPs were clearly fertility-related, aligning with field fertility in heat maps and PCA plots (Figs 2 - 4), and when these DAPs that were identified in the 6 bulls with extreme fertility were tested against the whole 16-bull cohort, many of them significantly correlated with the population's fertility (Table 3,4). The similar conclusions from two different types of statistical analyses affirmed the importance of these DAPS to fertility. Subsequent MCODE analysis provided insights into their roles and impact in sperm membrane pathways important to normal capacitation and fertilization, including energy production, motility, capacitation, acrosome reaction, and sperm-oocyte binding (Table 1), aligning with generic sperm quality measures attributed to some of these proteins (e.g., structure, metabolism, motility, capacitation, sperm-oocyte binding [4, 16]).

DAPs in high-fertility HPM such as L-lactate dehydrogenase A chain (Fig 5 and Table 3) and spermatogenesis-associated protein 19 (SPATA19) have been associated with energy and mitochondrial regulation [21, 22], reflecting the necessity of proper energy management for fertilization processes. The HPM is highly enriched in the head plasma membrane compared to whole sperm [20], although both HPM and whole sperm having components and functions in common, since normal fertility obviously requires common cytoskeletal and structural proteins. SPATA19's presence in the HPM may either be due to the small amount of mitochondrial membrane in HPM [20] or reflect the actual presence of SPATA19 in the plasma membrane of the sperm head; confirmation of location and elucidation of its significant positive association with *in vivo* fertility would be interesting to pursue. The down-regulated DAP

disintegrin and metalloprotease 32 (ADAM 32), one of the ADAM family of membrane-anchored proteins likely affecting cellular pathways, appeared to have a mild negative effect on fertility (Table 4) but did not impact male mouse fertility [23]. While a number of down-regulated DAPs like nucleoside diphosphate kinase homolog 5 (NME5) with its likely HPM role controlling antioxidant enzymes that protected sperm membrane lipids from peroxidative damage [24], tended to negatively correlate with *in vivo* fertility (Table 4), any negative effects must be compensable, possibly through the extensive PPI networks (e.g., Fig 6 a) providing alternate controls.

Since sperm and membrane structure and dynamics inter-relate, involve cytoskeletal elements impacting both flagellar motility and membrane structure and are critically important for fertility [25], [26], it was expected that proteins involved in both motility and microtubule structure and assembly would be found in HPM. The DAPs DNAI1, RSPH6A, RIBC2, and SPATA19 were in higher abundance (Fig 5) in HF bulls, indicating why mutation or absence of one or more of their genes caused sperm abnormalities and infertility [27]. Similarly the HF-increased DAPs actin capping proteins CAPZB, dynein DNAI1, and the microtubule protein RIB43A-like with coiled-coils protein 2 (RIBC2) that were significantly positively correlated with *in vivo* fertility (Table 3) have previously been noted as cytoskeletal elements causing dynamic HPM changes in capacitation and their absence was associated with various sperm abnormalities [27], [28].

Sperm capacitation is a series of complex membrane-directed processes involving molecular re-organisations and signalling that induce changes in sperm structure and function. Capacitation is initially triggered [11, 29, 30] by incompletely-understood signals from different sources that activate signaling pathways which ultimately stimulate onset of AE. Clustering analysis provided insights into the mechanisms and

pathways linking DAPs with capacitation. For example, the DAP acrosin binding protein (ACRBP) that was significantly correlated with *in vivo* fertility (Table 3) and was involved in capacitation [30], clustered with heat shock protein (HSP4L) and non-DAPs (Fig 5 c) like triosephosphate isomerase (TPI1), tyrosine-protein phosphatase (TPTE), atlastin-2 (ATL2) and succinate CoA ligase. ACRBP could impact capacitation through biochemical interactions with its clustered proteins, including TCP11 that facilitated the influx of calcium ions into the sperm head through calcium-dependent signaling pathways inducing capacitation and the AE [31]. In addition, TCP11 possibly interacted with TPTE and its signal transduction pathways [31], impacting cAMP-dependent signaling and ion transport. One cluster of HF-increased DAPs, ATP synthase F(0) complex subunit B1 (ATP5F1-Fig 5 m) and ATP synthase subunit d (ATP5H-Fig 5 l), were significantly correlated with BFI (Table 3) and formed networks (Fig 5) with non-DAPS such as AK5, AK7, ATP5D, ATP5J2, NT5C1A, NT5C1B, NME4 and NME8; these interactions influence the generation of ATP from ATP synthase while adenylate kinase interconverts adenine nucleosides [32, 33]. Again, deeper elucidation of the exact roles and components of the HPM pathways in capacitation that are newly-identified here (specifically, ATP synthesis pathway, adenylate kinase pathway, nucleotide metabolism pathway, nucleoside diphosphate kinase activity and calcium signaling pathways) could help understand critical controls of fertilization, since they are interconnected and collectively regulate sperm fertility by contributing to energy production, nucleotide metabolism, and signalling necessary for sperm motility, capacitation, and ultimately, successful fertilization in the sperm HPM.

Sperm fertility could be impacted by the actions of one or more of the HF-decreased DAPs that significantly inhibit fertilization: $Na^+/K^+$-ATPase α4, protein C9orf131

homolog, maestro heat-like repeat-containing protein family member 2B and mitochondrial chaperone BCS1. $Na^+/K^+$-ATPase α4's subnetwork (Fig 10 a) interacted with its non-DAP isoforms $Na^+/K^+$-ATPase α2 and $Na^+/K^+$-ATPase α3 that may complement or inhibit α4's effects. $Na^+/K^+$-ATPase α4 is most abundant in sperm tail where it is thought to stimulate motility and hyperactivation, supporting fertility [34]. Since α4 in the HPM correlated significantly with reduced fertility, α4 in the head membrane must interfere with normal capacitation, perhaps by interacting or competing with other α isoforms and misdirecting their signalling or transport activities. The cAMP-dependent PKA alpha was also negatively correlated with fertility and its isoform cAMP PKA gamma clustered with α4 ATPase, perhaps suggesting that competition between the two PKA isoforms, and between the ATPase isoforms, impacts normal capacitation and fertilization. This identification of specific HPM proteins with critical roles will facilitate untangling pathways and roles in energy, transporting, and/or signaling to identify the critical one(s) for fertilization.

Similar to α4 ATPase, the DAP ROPN1L previously was associated with axoneme integrity and sperm hyperactivation and PKA signalling pathway [35-37], but unlike α4, ROPN1L in the HPM was associated with improved fertility (Table 3). This most likely involved PKA, since ROPN1L clustered with the DAP AKAP3 (Fig 5 a, b) that induced signaling complexes [38]. Activating the proper PKA signalling pathway may be crucial for effective capacitation, as while greater amounts of ROPN1L supported fertility, greater amounts of the HF-decreased DAP maestro heat-like repeat family member 2B (MROH2B) lowered BFI (Table 4), presumably through its known stimulation of excessive PKA signalling, premature capacitation and reduced fertility [39, 40]. Thus ROPN1L, AKAP3, and MROH2B all point to the crucial nature of HPM-

linked PKA signalling as a critically important control point in capacitation and fertilization.

Another potential molecular pair of DAPs may impact HPM-related fertility through substitution or competition, as proposed for the ATPases and PKAs. RAB2B was significantly increased in HF while RAB2A tended (p=0.07) to be HF-decreased and many other non-DAP members of the RAB family clustered together in HPM (Fig 6 b: RAB10, 14, 37, 39A, 43). RABs are small GTP-ases of approximately 20–40 kDa [41]; RAB2B was depleted in humans with unexplained fertilization failure [42], RAB2A regulated vesicular transport to the developing acrosome during spermiogenesis [43], and various RABs regulated capacitation-like physiological changes such as calcium release, EGFR interaction, regulation of phosphatidyl-inositol 3P levels [44] and membrane transport [45]. The interactions of the DAPs, both those in higher and lower abundance in HF versus LF, and their interactions with those HPM proteins with which they cluster, are complex but clearly important to successful capacitation and fertilization.

The increased abundance of the antioxidant enzyme phospholipid hydroperoxide glutathione peroxidase in the HPM of HF bulls (GPX4; Fig 5 k) correlated positively with the population fertility. GPX4 prevented peroxidative damage of membrane lipids [46] and prevented reactive oxygen species (ROS) from changing a cAMP-driven Tyr-P pathway [47] needed for capacitation. GPX4 has also been found in sperm from high fertility bulls [48] and in human sperm anterior membranes and post-acrosomal membranes [48]; it maintained cytoskeletal integrity [49] and was involved in fertilization [50]. It is interesting that MCODE linked GPX4 to lactate dehydrogenase A (LDHA; Fig 8), which was noted as a possible male contraceptive

[51]. Therefore membrane-bound dehydrogenase and peroxidase may be inter-related in control of sperm fertility.

Sperm-oocyte binding is a multi-step function of the HPM, and a number of DAPs implicated in these processes were identified (Fig 5). Several of the HF-increased DAPs ACRBP and HSPA4L and the non-DAPs in their clusters [zona pellucida-binding protein 1 (ZPBP1), ZPBP2, zonadhesin (ZAN) [65], acrosin (ACR), epididymal sperm-binding protein 1 (ELSPBP1), mitochondrial (SUCLA2), ODF1, ROPN1] have possible roles in AE and sperm-oocyte interactions. ACRBP was elevated in capacitated boar spermatozoa, stimulated release of acrosin from the acrosome and sperm-egg binding and was suggested as a potential biomarker of fertility [60]. Clustering ACRBP with ZPBP2, ZPBP1, ACR, ZAN mediated sperm-ZP interactions [52] and absence of ZPBP2's caused male subfertility due to defects in sperm-ZP interactions [53].

Thus, HPM proteins identified here play roles in every aspect of the dynamic sperm membrane changes that initiate and control capacitation, sperm-oocyte binding, and fertilization.



## Conclusions

This first meticulous in-depth proteomics analysis of sperm HPM in Holstein Friesian bulls found their rigorously measured field fertility significantly correlated to the amount of DAPs identified by mass spectrometry-based proteomics analysis. Of the over 20,000 proteins identified, only 67 differed by at least two-fold between high and low fertility bulls, with over 40 of these proteins significantly correlated to the wide range of *in vivo* fertility of 16 bulls. This unique identified orchestra of proteins participated in various key roles in sperm motility, capacitation, oocyte recognition,

metabolism, signaling pathways and cytoskeletal structure, and overall cast light on the proteins that regulate bovine sperm fertility.

## Materials and Methods

### Semen

Fresh double ejaculates were obtained from 16 Holstein Friesian bulls (semen was gifted by Semex, Guelph, ON, Canada) with known field fertility, classified as average-to-high fertility (ATH, BFI > 100; n = 8) and average-to-low fertility (ATL, BFI < 100; n = 8) based on the international multi-factor BFI. The BFI is a Semex-calculated metric using NRR, sire conception rate, and Agri-Tech analyses, with an average BFI set at 100 based on >1000 inseminations per bull from several hundred bulls. Two ejaculates were collected from each bull, combined, and those with ≥80% motile sperm were diluted to $60\times10^6$ spermatozoa per mL using egg yolk-free extender. The samples were shipped to our laboratory at the University of Saskatchewan, and their temperature was adjusted to room temperature (24 ± 1 ºC) upon arrival. A 500 µL aliquot was then incubated at 37 ºC for gradual warming and evaluated for motility kinetics using CASA Hamilton Thorne IVOS II (MA, USA). Ejaculates meeting 15-20 ºC temperature and demonstrating CASA motility were processed to obtain HPM once the ejaculate reached room temperature [19].



### Reagents and Equipment

Disodium phosphate, sodium dihydrogen phosphate monohydrate, dextrose, 1.5 M sucrose, polyethylene glycol (40%), methanol HPLC grade, and trypsin were purchased from Thermo-Fisher Scientific (Unionville, ON, Canada) and percoll from GE Healthcare (Mississauga, ON, Canada). Potassium chloride, 20% dextran, sodium chloride were acquired from Sigma-Aldrich, (Oakville, ON, Canada). Milli-Q water

obtained from water purification system Serv A Pure (MIUS) and MS-SAFE protease and phosphatase inhibitor cocktail from Merck KGaA (Darmstadt, Germany). Bicinchoninic acid protein assay kit including BSA were purchased from Thermo Fisher Scientific (Waltham, MA, USA). LC/MS grade water, and LC/MS grade acetonitrile, were purchased from Fisher Scientific, (Fair Lawn, NJ, USA), as were ammonium bicarbonate (ABC) buffer, trifluoroethanol (TFE) and iodoacetamide (IAA). Dithiothreitol (DTT) was purchased from MP Biomedicals (Solon, OH, USA). Strong cation exchange (SCX) Spin Tips sample preparation kit was purchased from Protea Biosciences (Morgantown, WV, USA), ammonium formate from Sigma (St. Louis, MO, USA) and trypsin from Pierce (Rockford, IL, USA). MS vials and Polaris-HR-Chip 3C18 were purchased [19] from Agilent (Agilent Technologies Canada Ltd., Mississauga, ON, CA).

## Isolation of Sperm HPM

The HPM was obtained according to an established procedure [19, 20, 54, 55], performing all steps at room temperature unless specified otherwise. Briefly, the sample was centrifuged (Jouan CT 4.22; Jouan S.A., Saint-Herblain, France; 800 x g; 10 min), and pellets resuspended into phosphate buffered saline (PBS; 125 mM NaCl, 8 mM $Na_2HPO_4$, 2 mM $NaH_2PO_4.H_2O$, 5 mM KCl, 5 mM dextrose) with repeated gentle aspiration, pooled to ~40 mL and centrifuged (800 x g; 10 min). The resulting pellets were resuspended in PBS to 40 mL, layered onto 35% percoll (1:2 v:v; percoll:PBS) centrifuged (800 x g; 10 min), the supernatant discarded, and the pellet washed twice with PBS (800 x g, 10 min). The final pellet was subjected to nitrogen cavitation in a cell disruption Parr cavitation unit (Parr instrument company, IL, USA) introducing nitrogen gas over 90 sec to a final pressure of 650 psi, holding for 10 min and then releasing pressure over 90 sec. Finally, the cavitate was centrifuged at 800 x g for 10

min. Phase partition tubes were prepared by mixing 3.94 g 20% dextran (1:5 g:g; dextran:water), 1.97 g 40 % PEG (1:2.5 g:g; PEG:water), 0.19 g PBS (in 1000 mL water), 2.42 g 1.5 M sucrose (in 100 mL water), covering and keeping in fridge overnight. The resulting supernatant was layered onto four phase partition tubes. Tubes were mixed by inversion 20 times, centrifuged (800 x g; 10 min), and the top portion harvested. This portion was layered onto four fresh phase partition tubes, mixed, and centrifuged as before. The final top layers were centrifuged (206,000 x g; 30 min; 5 ºC), the pellets resuspended in PBS, pooled, and centrifuged (206,000 x g; 20 min; 5 ºC). The final pellet (HPM) was scraped out into a hand-held homogenizer by stepwise adding 200 µL PBS, and homogenized. To inactivate endogenous proteolytic and phospholytic enzymes that degrade the HPM proteins, and their activation states, MS-SAFE protease and phosphatase inhibitor cocktail was added (1.33 mL per mg of HPM). The samples were homogenized, aliquoted into Eppendorf tubes, covered with nitrogen gas, snap frozen in liquid nitrogen, and stored at -80 ºC [19].



**Protein Digestion**

HPM protein concentration was determined by bicinchoninic acid analysis using the BioTek ELx808 (BioTek- Instruments Inc., VT, USA) multi detection plate reader (wavelength 562 nm) and BSA as the standard protein [19, 56]. Triplicates from each HPM were digested into peptides using in-solution trypsin digestion protocol [57]. Briefly, samples were normalized at a concentration of 5.0 µg/µL using ABC buffer. Protein denaturation was achieved with TFE. Disulfide bonds were reduced using DTT, followed by alkylation with IAA. After drying and removal of impurities, samples were resuspended in ABC and digested with trypsin [19]. The digestion process was

completed the next morning, and samples were dried and stored at -80 ºC for subsequent SCX fractionation [19, 57].

## Strong Cation Exchange Peptide Fractionation

Peptide fractionation using SCX Spin Tips was incorporated to enhance sample resolution prior to MS/MS analysis [19, 57, 58]. From each animal's HPM, 9 fractions were acquired. Briefly, the SCX Spin Tip column was conditioned, trypsin-digested HPM peptides reconstituted in 100-200 µL of SCX reconstitution solution (pH < 3, adjusted with formic acid), loaded on the SCX Spin Tip column, and centrifuged at 4000 x g for 6 min [19]. The Spin Tip column was then eluted using a solution of ammonium formate in 10% acetonitrile in stepwise increasing strength (20, 40, 60, 80, 100, 150, 250 and 500 mM, respectively; 150 µL each; pH ~ 3). A total of 9 fractions, including the flow through fraction, were acquired and stored at -80 ºC until MS analysis [19, 58, 59].

## Tandem Mass Spectrometry Analysis

Dried SCX fractions containing tryptic peptides were vortexed, centrifuged, and subjected to LC-MS/MS analysis. An Agilent 6550 iFunnel Q-TOF mass spectrometer (Agilent Technologies, Mississauga, ON, CA) coupled with liquid chromatography instrumentation [60] was used (Agilent Technologies, Mississauga, ON, CA) [19, 60]. Reversed phase chromatographic separation of peptides was achieved by employing an Agilent HPLC-Chip; G4240-62030 chip cube, Polaris-HR-Chip 3C18 containing a 360 nL enrichment column and a 75 µm × 150 mm analytical column (Agilent Technologies, Mississauga, ON, CA); both columns were packed with Polaris C18, 180Å, 3 µm stationary phase for improved peptide resolutions and peak capacity. Peptide fractions were loaded onto the enrichment column with a specific solvent composition, followed by separation on the analytical column using a linear gradient

program. Mass spectra were acquired in positive ion mode with defined parameters, including mass range and scan rate [19]. Auto MS/MS was performed with a set threshold for precursor ion selection and exclusion [19, 57, 60].

## Database Search and Analysis

MS/MS spectra were obtained and searched against a *Mammals* species protein database (Swiss Prot, UniProt release 2020_06) using the Agilent Spectrum Mill search engine. The search parameters included trypsin as the enzyme for protein digestion, specific cleavage rules, and fixed modification of cysteine (carbamidomethylation). Variable modifications were applied in four stages, incorporating various post-translational modifications. Validated hits from each stage were used for subsequent searches [19]. The Spectrum Mill validation was performed at both peptide and protein levels with 1% FDR and peptide sequence length [57]. Furthermore, each identified DAP underwent manual validation using MassHunter software with a mass difference cutoff $\Delta m < 10$ PPM to ensure accuracy. A comparison was made between the identified proteins in ATH ($n = 8$) and ATL ($n = 8$) bulls. Proteins present in both groups were categorized as common proteins, while proteins exclusive to one group were considered unique to that fertility group [19].



## Statistical Analysis and Protein Network Analysis

For this study, three bulls with the highest BFI were labeled as high fertility (HF; BFI of 105,105,107), and three with the lowest BFI were designated as low fertility (LF; BFI of 88,92,94). HF and LF were statistically compared with t-tests using MPP software; statistical rigour was enhanced by applying the Benjamini and Hochberg correction with an FDR threshold of $< 1\%$, and a p-value cutoff of $< 0.05$. Proteins were classified as increased or decreased in HF relative to LF based on a fold change of $\geq 2$ in spectral intensities between the compared groups. The resulting 67

differentially abundant proteins were manually validated using Mass Hunter software [19].

To enhance data interpretation, accession numbers of significant DAPs from multiple species were converted into homologous proteins of *Homo sapiens* for further protein-protein interaction (PPI) and networking analysis. Subnetworks of HF-increased or HF-decreased DAPs with all identified non-differentially abundant proteins (non-DAPs) in high-fertility HPM were constructed using Cytoscape. PPI networks among DAPs were generated through STRING analysis, which provides known and predicted PPI. A Cytoscape analysis was performed to construct a complete interactome of HPM. The most significant clusters within the DAPs' STRING PPI networks were identified using the molecular complex detection (MCODE) plugin in Cytoscape [19].

Linear regression analysis was conducted with SAS statistical software (SAS; version 9.3; SAS Institute, Inc Cary, NC) on the intensities of the DAPs relative to BFI. The analysis was first performed for the HF and LF groups (n = 3 per group) and then for the entire population [19] of bulls (n = 16). The deterministic model used was $y = a + bx$, where a = intercept and b = slope of the regression line.



## Data Availability

The mass spectrometry proteomics data have been deposited to the ProteomeXchange Consortium via the PRIDE partner repository [61] with the dataset identifier PXD047294 and are available from the corresponding author on reasonable request.

## Credit authorship contribution statement

**Muhammad Imran:** contributed to conceptualization, experimental design, conducted the study, performed data analysis, validation, visualization, wrote first draft of manuscript and revised. **Mary M. Buhr:** contributed to conceptualization, funding acquisition, project administration, resources, supervision and manuscript revision and final approval. **Paulos Chumala:** contributed to acquiring MS data and data analysis. **George S. Katselis:** contributed to conceptualization of the experimental design, funding acquisition, project administration, supervision, resources and manuscript revision and final approval.

## Declaration of Competing Interest

The authors declare that they have no known competing financial interests or personal relationships that could have appeared to influence the work reported in this paper.



---

## Acknowledgments

Research reported in this publication was supported by NSERC for funding and Semex in Guelph Ontario provided gift of semen and bull fertility analysis. Canadian Centre for Rural and Agricultural Health provided Founding Chairs Fellowship award to the first author and support for the MS instrumentation.

## Abbreviations:

ACRBP: Acrosin Binding Protein
ADAM: A Disintegrin And Metalloproteinase
AE: Acrosomal Exocytosis
AI: Artificial Insemination
AK5: Adenylate Kinase 5
AK7: Adenylate Kinase 7
AKAP3: A-Kinase Anchoring Protein 3
ATL2: Atlastin-2
ATP: Adenosine Triphosphate

ATP5D: ATP Synthase Subunit d
ATP5F1: ATP Synthase F(0) Complex Subunit B1
ATP5H: ATP Synthase Subunit d
ATP5J2: ATP Synthase Subunit d
BFI: Bull Fertility Index
CASA: Computer-Assisted Sperm Analysis
DAPs: Differentially Abundant Proteins
DNAI1: Dynein Axonemal Intermediate Chain 1
ELSPBP1: Epididymal Sperm-Binding Protein 1
FDR: False Discovery Rate
GO: Gene Ontology
GPX4: Glutathione Peroxidase 4
HF: High Fertility
HPM: High-Performance Membrane
LC/MS: Liquid Chromatography/Mass Spectrometry
LC-MS/MS: Liquid Chromatography-Mass Spectrometry/Mass Spectrometry
LF: Low Fertility
LDHA: L-Lactate Dehydrogenase A Chain
MPP: Mass Profiler Professional
MCODE: Molecular Complex Detection
MS: Mass Spectrometry
ND: No Data/Not Detected
NME5: Non-Metastatic Cells 5, Protein Expressing
NRR: Non-Return Rate
NT5C1A: 5'-Nucleotidase, Cytosolic IA
NT5C1B: 5'-Nucleotidase, Cytosolic IB
OGC: Observed Gene Count
ODF1: Outer Dense Fiber Protein 1
PATHER: Pathway Analysis Through Hidden Entities and Relationships
PCA: Principal Component Analysis
PKA: Protein Kinase A
PPI: Protein-Protein Interaction
RAB2A: Ras-Related Protein Rab-2A
RAB2B: Ras-Related Protein Rab-2B
RIBC2: RIB43A-Like With Coiled-Coils Protein 2
ROPN1L: Rhophilin Associated Tail Protein 1-Like
ROS: Reactive Oxygen Species
RSPH6A: Radial Spoke Head Component 6 Homolog A
SPATA19: Spermatogenesis-Associated Protein 19
STRING: Search Tool for the Retrieval of Interacting Genes/Proteins
SUCLA2: Succinate-CoA Ligase ADP-Forming Subunit Beta
TPI1: Triosephosphate Isomerase
TPTE: Tyrosine-Protein Phosphatase
UniProt: Universal Protein Resource
UniProtKB: Universal Protein Resource Knowledgebase
ZAN: Zonadhesin
ZPBP1: Zona Pellucida-Binding Protein 1
ZPBP2: Zona Pellucida-Binding Protein 2

## References


1. Amann, R. P., Saacke, R. G., Barbato, G. F. & Waberski, D. (2018). Measuring Male-to-Male Differences in Fertility or Effects of Semen Treatments. Annual Review of Animal Biosciences. **6**, 255-286. https://doi.org/10.1146/annurev-animal-030117-014829.
2. Graham, J. K. & Mocé, E. (2005). Fertility evaluation of frozen/thawed semen. Theriogenology. **64**, 492-504. https://doi.org/10.1016/j.theriogenology.2005.05.006.
3. Watson, P. F. (2000). The causes of reduced fertility with cryopreserved semen. Animal Reproduction Science. **60-61**, 481-492. https://doi.org/10.1016/S0378-4320(00)00099-3.
4. D'Amours, O., Frenette, G., Bourassa, S., Calvo, É., Blondin, P. & Sullivan, R. (2018). Proteomic Markers of Functional Sperm Population in Bovines: Comparison of Low- and High-Density Spermatozoa Following Cryopreservation. Journal of Proteome Research. **17**, 177-188. https://doi.org/10.1021/acs.jproteome.7b00493.
5. Butler, M. L., Bormann, J. M., Weaber, R. L., Grieger, D. M. & Rolf, M. M. (2020). Selection for bull fertility: a review. Translational Animal Science. **4**, 423-441. https://doi.org/10.1093/tas/txz174.
6. Tahmasbpour, E., Balasubramanian, D. & Agarwal, A. (2014). A multi-faceted approach to understanding male infertility: gene mutations, molecular defects and assisted reproductive techniques (ART). Journal of Assisted Reproduction and Genetics. **31**, 1115-1137. https://doi.org/10.1007/s10815-014-0280-6.
7. Kasimanickam, R. K., Kasimanickam, V. R., Arangasamy, A. & Kastelic, J. P. (2019). Sperm and seminal plasma proteomics of high- versus low-fertility Holstein bulls. Theriogenology. **126**, 41-48. https://doi.org/10.1016/j.theriogenology.2018.11.032.
8. Sudano, M. J., Crespilho, A. M., Fernandes, C. B., Junior, A. M., Papa, F. O., Rodrigues, J., Machado, R. & Landim-Alvarenga, F. D. C. (2011). Use of bayesian inference to correlate in vitro embryo production and in vivo fertility in Zebu Bulls. Veterinary Medicine International. **2011**, 1-6. https://doi.org/10.4061/2011/436381.
9. Peddinti, D., Nanduri, B., Kaya, A., Feugang, J. M., Burgess, S. C. & Memili, E. (2008). Comprehensive proteomic analysis of bovine spermatozoa of varying fertility rates and identification of biomarkers associated with fertility. BMC Systems Biology. **2**, 19-19. https://doi.org/10.1186/1752-0509-2-19.
10. M. K, M. A., Kumaresan, A., Yadav, S., Mohanty, T. K. & Datta, T. K. (2019). Comparative proteomic analysis of high- and low-fertile buffalo bull spermatozoa for identification of fertility-associated proteins. Reproduction in Domestic Animals. **54**, 786-794. https://doi.org/10.1111/rda.13426.
11. Awda, B. J., Mahoney, I. V., Pettitt, M., Imran, M., Katselis, G. S. & Buhr, M. M. (2023). Existence and importance of Na(+)K(+)-ATPase in the plasma membrane of boar spermatozoa. Can J Physiol Pharmacol. https://doi.org/10.1139/cjpp-2023-0116.
12. Singh, R., Sengar, G. S., Singh, U., Deb, R., Junghare, V., Hazra, S., Kumar, S., Tyagi, S., Das, A. K., Raja, T. V. & Kumar, A. (2018). Functional proteomic analysis of crossbred (Holstein Friesian × Sahiwal) bull spermatozoa. Reproduction in Domestic Animals. **53**, 588-608. https://doi.org/10.1111/rda.13146.

13. Viana, A. G. A., Martins, A. M. A., Pontes, A. H., Fontes, W., Castro, M. S., Ricart, C. A. O., Sousa, M. V., Kaya, A., Topper, E., Memili, E. & Moura, A. A. (2018). Proteomic landscape of seminal plasma associated with dairy bull fertility. Scientific Reports. **8**, 16323-16323. https://doi.org/10.1038/s41598-018-34152-w.
14. Somashekar, L., Selvaraju, S., Parthipan, S., Patil, S. K., Binsila, B. K., Venkataswamy, M. M., Karthik Bhat, S. & Ravindra, J. P. (2017). Comparative sperm protein profiling in bulls differing in fertility and identification of phosphatidylethanolamine-binding protein 4, a potential fertility marker. Andrology. **5**, 1032-1051. https://doi.org/10.1111/andr.12404.
15. Muhammad Aslam, M. K., Sharma, V. K., Pandey, S., Kumaresan, A., Srinivasan, A., Datta, T. K., Mohanty, T. K. & Yadav, S. (2018). Identification of biomarker candidates for fertility in spermatozoa of crossbred bulls through comparative proteomics. Theriogenology. **119**, 43-51. https://doi.org/10.1016/j.theriogenology.2018.06.021.
16. Byrne, K., Leahy, T., McCulloch, R., Colgrave, M. L. & Holland, M. K. (2012). Comprehensive mapping of the bull sperm surface proteome. PROTEOMICS. **12**, 3559-3579. https://doi.org/10.1002/pmic.201200133.
17. Gadella, B. M. & Boerke, A. (2016). An update on post-ejaculatory remodeling of the sperm surface before mammalian fertilization. Theriogenology. **85**, 113-124. https://doi.org/10.1016/j.theriogenology.2015.07.018.
18. Caballero, J., Frenette, G., D'Amours, O., Belleannee, C., Lacroix-Pepin, N., Robert, C. & Sullivan, R. (2012). Bovine sperm raft membrane associated Glioma Pathogenesis-Related 1-like protein 1 (GliPr1L1) is modified during the epididymal transit and is potentially involved in sperm binding to the zona pellucida. Journal of Cellular Physiology. **227**, 3876-3886. https://doi.org/10.1002/jcp.24099.
19. Imran, M. (2023). Identification and Quantification of Sperm Head Plasma Membrane Proteins Associated with Male Fertility. PhD Thesis, College of Graduate and Postdoctoral Studies pp. 258, University of Saskatchewan, Saskatoon, SK, Canada.
20. Zhao, Y. & Buhr, M. M. (1996). Localization of various ATPases in fresh and cryopreserved bovine spermatozoa. Animal Reproduction Science. **44**, 139-148. https://doi.org/10.1016/0378-4320(96)01547-3.
21. Mi, Y., Shi, Z. & Li, J. (2015). Spata19 is critical for sperm mitochondrial function and male fertility. Molecular Reproduction and Development. **82**, 907-913. https://doi.org/10.1002/mrd.22536.
22. Nourashrafeddin, S., Ebrahimzadeh-Vesal, R., Modarressi, M. H., Zekri, A. & Nouri, M. (2014). Identification of Spata-19 new variant with expression beyond meiotic phase of mouse testis development. Reports of biochemistry & molecular biology. **2**, 89-93.
23. Lee, S., Hong, S. H. & Cho, C. (2020). Normal fertility in male mice lacking ADAM32 with testis-specific expression. Reproductive Biology. **20**, 589-594. https://doi.org/10.1016/j.repbio.2020.09.001.
24. Munier, A., Feral, C., Milon, L., Pinon, V. P., Gyapay, G., Capeau, J., Guellaen, G. & Lacombe, M. L. (1998). A new human nm23 homologue (nm23-H5) specifically expressed in testis germinal cells. FEBS Lett. **434**, 289-294. https://doi.org/10.1016/s0014-5793(98)00996-x.
25. Zhou, J., Du, Y.-R., Qin, W.-H., Hu, Y.-G., Huang, Y.-N., Bao, L., Han, D., Mansouri, A. & Xu, G.-L. (2009). RIM-BP3 is a manchette-associated protein essential for

spermiogenesis. Development. **136**, 373-382. https://doi.org/10.1242/dev.030858.
26. Teves, M. E. & Roldan, E. R. S. (2022). Sperm bauplan and function and underlying processes of sperm formation and selection. Physiological Reviews. **102**, 7-60. https://doi.org/10.1152/physrev.00009.2020.
27. Whitfield, M., Thomas, L., Bequignon, E., Schmitt, A., Stouvenel, L., Montantin, G., Tissier, S., Duquesnoy, P., Copin, B., Chantot, S., Dastot, F., Faucon, C., Barbotin, A. L., Loyens, A., Siffroi, J.-P., Papon, J.-F., Escudier, E., Amselem, S., Mitchell, V., Touré, A. & Legendre, M. (2019). Mutations in DNAH17, Encoding a Sperm-Specific Axonemal Outer Dynein Arm Heavy Chain, Cause Isolated Male Infertility Due to Asthenozoospermia. The American Journal of Human Genetics. **105**, 198-212. https://doi.org/10.1016/j.ajhg.2019.04.015.
28. Vignjevic, D. & Montagnac, G. (2008). Reorganisation of the dendritic actin network during cancer cell migration and invasion. Seminars in Cancer Biology. **18**, 12-22. https://doi.org/10.1016/j.semcancer.2007.08.001.
29. Austin, C. R. (1952). The 'Capacitation' of the Mammalian Sperm. Nature. **170**, 326-326. https://doi.org/10.1038/170326a0.
30. Petit, F. M., Serres, C., Bourgeon, F., Pineau, C. & Auer, J. (2013). Identification of sperm head proteins involved in zona pellucida binding. Human Reproduction. **28**, 852-865. https://doi.org/10.1093/humrep/des452.
31. Chen, H., Rossier, C., Morris, M. A., Scott, H. S., Gos, A., Bairoch, A. & Antonarakis, S. E. (1999). A testis-specific gene, TPTE, encodes a putative transmembrane tyrosine phosphatase and maps to the pericentromeric region of human chromosomes 21 and 13, and to chromosomes 15, 22, and Y. Human Genetics. **105**, 399-409. https://doi.org/10.1007/s004399900144.
32. Tükenmez, H., Magnussen, H. M., Kovermann, M., Byström, A. & Wolf-Watz, M. (2016). Linkage between Fitness of Yeast Cells and Adenylate Kinase Catalysis. PLOS ONE. **11**, e0163115-e0163115. https://doi.org/10.1371/journal.pone.0163115.
33. Yu, J., Chen, B., Zheng, B., Qiao, C., Chen, X., Yan, Y., Luan, X., Xie, B., Liu, J., Shen, C., He, Z., Hu, X., Liu, M., Li, H., Shao, Q. & Fang, J. (2019). ATP synthase is required for male fertility and germ cell maturation in Drosophila testes. Molecular Medicine Reports. https://doi.org/10.3892/mmr.2019.9834.
34. Rajamanickam, G. D., Kastelic, J. P. & Thundathil, J. C. (2017). Content of testis-specific isoform of Na/K-ATPase (ATP1A4) is increased during bovine sperm capacitation through translation in mitochondrial ribosomes. Cell and Tissue Research. **368**, 187-200. https://doi.org/10.1007/s00441-016-2514-7.
35. Chen, J., Wang, Y., Wei, B., Lai, Y., Yan, Q., Gui, Y. & Cai, Z. (2011). Functional Expression of Ropporin in Human Testis and Ejaculated Spermatozoa. Journal of Andrology. **32**, 26-32. https://doi.org/10.2164/jandrol.109.009662.
36. Zhao, W., Li, Z., Ping, P., Wang, G., Yuan, X. & Sun, F. (2018). Outer dense fibers stabilize the axoneme to maintain sperm motility. Journal of Cellular and Molecular Medicine. **22**, 1755-1768. https://doi.org/10.1111/jcmm.13457.
37. Xu, K., Yang, L., Zhang, L. & Qi, H. (2020). Lack of AKAP3 disrupts integrity of the subcellular structure and proteome of mouse sperm and causes male sterility. Development. **147**. https://doi.org/10.1242/dev.181057.
38. Li, Y.-F., He, W., Mandal, A., Kim, Y.-H., Digilio, L., Klotz, K., Flickinger, C. J., Herr, J. C. & Herr, J. C. (2011). CABYR binds to AKAP3 and Ropporin in the human sperm fibrous sheath. Asian Journal of Andrology. **13**, 266-274. https://doi.org/10.1038/aja.2010.149.

39. Martin-Hidalgo, D., Macias-Garcia, B., Garcia-Marin, L. J., Bragado, M. J. & Gonzalez-Fernandez, L. (2020). Boar spermatozoa proteomic profile varies in sperm collected during the summer and winter. Anim Reprod Sci. **219**, 106513. https://doi.org/10.1016/j.anireprosci.2020.106513.
40. Bechtel, S., Rosenfelder, H., Duda, A., Schmidt, C. P., Ernst, U., Wellenreuther, R., Mehrle, A., Schuster, C., Bahr, A., Blocker, H., Heubner, D., Hoerlein, A., Michel, G., Wedler, H., Kohrer, K., Ottenwalder, B., Poustka, A., Wiemann, S. & Schupp, I. (2007). The full-ORF clone resource of the German cDNA Consortium. BMC Genomics. **8**, 399. https://doi.org/10.1186/1471-2164-8-399.
41. Lin, Y.-H., Ke, C.-C., Wang, Y.-Y., Chen, M.-F., Chen, T.-M., Ku, W.-C., Chiang, H.-S. & Yeh, C.-H. (2017). RAB10 Interacts with the Male Germ Cell-Specific GTPase-Activating Protein during Mammalian Spermiogenesis. International Journal of Molecular Sciences. **18**, 97-97. https://doi.org/10.3390/ijms18010097.
42. Torra-Massana, M., Jodar, M., Barragán, M., Soler-Ventura, A., Delgado-Dueñas, D., Rodríguez, A., Oliva, R. & Vassena, R. (2021). Altered mitochondrial function in spermatozoa from patients with repetitive fertilization failure after ICSI revealed by proteomics. Andrology. **9**, 1192-1204. https://doi.org/10.1111/andr.12991.
43. Mountjoy, J. R., Xu, W., McLeod, D., Hyndman, D. & Oko, R. (2008). RAB2A: A Major Subacrosomal Protein of Bovine Spermatozoa Implicated in Acrosomal Biogenesis1. Biology of Reproduction. **79**, 223-232. https://doi.org/10.1095/biolreprod.107.065060.
44. Nassari, S., Del Olmo, T. & Jean, S. (2020). Rabs in Signaling and Embryonic Development. International Journal of Molecular Sciences. **21**, 1064-1064. https://doi.org/10.3390/ijms21031064.
45. Stenmark, H. (2009). Rab GTPases as coordinators of vesicle traffic. Nature Reviews Molecular Cell Biology. **10**, 513-525. https://doi.org/10.1038/nrm2728.
46. Cho, E. H., Huh, H. J., Jeong, I., Lee, N. Y., Koh, W. J., Park, H. C. & Ki, C. S. (2020). A nonsense variant in NME5 causes human primary ciliary dyskinesia with radial spoke defects. Clinical Genetics. **98**, 64-68. https://doi.org/10.1111/cge.13742.
47. Awda, B. J. & Buhr, M. M. (2010). Extracellular Signal-Regulated Kinases (ERKs) Pathway and Reactive Oxygen Species Regulate Tyrosine Phosphorylation in Capacitating Boar Spermatozoa1. Biology of Reproduction. **83**, 750-758. https://doi.org/10.1095/biolreprod.109.082008.
48. Özbek, M., Hitit, M., Kaya, A., Jousan, F. D. & Memili, E. (2021). Sperm Functional Genome Associated With Bull Fertility. Frontiers in Veterinary Science. **8**. https://doi.org/10.3389/fvets.2021.610888.
49. Maiorino, M., Roveri, A., Benazzi, L., Bosello, V., Mauri, P., Toppo, S., Tosatto, S. C. E. & Ursini, F. (2005). Functional Interaction of Phospholipid Hydroperoxide Glutathione Peroxidase with Sperm Mitochondrion-associated Cysteine-rich Protein Discloses the Adjacent Cysteine Motif as a New Substrate of the Selenoperoxidase. Journal of Biological Chemistry. **280**, 38395-38402. https://doi.org/10.1074/jbc.M505983200.
50. Rahman, M. S., Lee, J.-S., Kwon, W.-S. & Pang, M.-G. (2013). Sperm Proteomics: Road to Male Fertility and Contraception. International Journal of Endocrinology. **2013**, 1-11. https://doi.org/10.1155/2013/360986.

51. Goldberg, E. (2021). The sperm-specific form of lactate dehydrogenase is required for fertility and is an attractive target for male contraception (a review). Biology of Reproduction. **104**, 521-526. https://doi.org/10.1093/biolre/ioaa217.
52. Lin, Y.-N., Roy, A., Yan, W., Burns, K. H. & Matzuk, M. M. (2007). Loss of Zona Pellucida Binding Proteins in the Acrosomal Matrix Disrupts Acrosome Biogenesis and Sperm Morphogenesis. Molecular and Cellular Biology. **27**, 6794-6805. https://doi.org/10.1128/MCB.01029-07.
53. Ferrer, M., Cornwall, G. & Oko, R. (2013). A Population of CRES Resides in the Outer Dense Fibers of Spermatozoa1. Biology of Reproduction. **88**. https://doi.org/10.1095/biolreprod.112.104745.
54. Buhr, M. M., Curtis, E. F., Thompson, J. A., Wilton, J. W. & Johnson, W. H. (1993). Diet and breed influence the sperm membranes of beef bulls. Theriogenology. **39**, 581-592. https://doi.org/10.1016/0093-691x(93)90245-z.
55. Hickey, K. D. & Buhr, M. M. (2012). Characterization of Na+K+-ATPase in bovine sperm. Theriogenology. **77**, 1369-1380. https://doi.org/10.1016/j.theriogenology.2011.10.045.
56. Nair, M., Jagadeeshan, S., Katselis, G., Luan, X., Momeni, Z., Henao-Romero, N., Chumala, P., Tam, J. S., Yamamoto, Y., Ianowski, J. P. & Campanucci, V. A. (2021). Lipopolysaccharides induce a RAGE-mediated sensitization of sensory neurons and fluid hypersecretion in the upper airways. Scientific Reports. **11**, 8336-8336. https://doi.org/10.1038/s41598-021-86069-6.
57. Koziy, R. V., Bracamonte, J. L., Yoshimura, S., Chumala, P., Simko, E. & Katselis, G. S. (2022). Discovery proteomics for the detection of putative markers for eradication of infection in an experimental model of equine septic arthritis using LC-MS/MS. Journal of Proteomics. **261**, 104571-104571. https://doi.org/10.1016/j.jprot.2022.104571.
58. Mirzaei, H. & Regnier, F. (2006). Enrichment of Carbonylated Peptides Using Girard P Reagent and Strong Cation Exchange Chromatography. Analytical Chemistry. **78**, 770-778. https://doi.org/10.1021/ac0514220.
59. Creese, A. J., Shimwell, N. J., Larkins, K. P. B., Heath, J. K. & Cooper, H. J. (2013). Probing the Complementarity of FAIMS and Strong Cation Exchange Chromatography in Shotgun Proteomics. Journal of the American Society for Mass Spectrometry. **24**, 431-443. https://doi.org/10.1007/s13361-012-0544-2.
60. Henry, M., Coleman, O., Prashant, Clynes, M. & Meleady, P. (2017). Phosphopeptide Enrichment and LC-MS/MS Analysis to Study the Phosphoproteome of Recombinant Chinese Hamster Ovary Cells. Methods in molecular biology (Clifton, N.J.). **1603**, 195-208. https://doi.org/10.1007/978-1-4939-6972-2_13.
61. Vizcaino, J. A., Cote, R. G., Csordas, A., Dianes, J. A., Fabregat, A., Foster, J. M., Griss, J., Alpi, E., Birim, M., Contell, J., O'Kelly, G., Schoenegger, A., Ovelleiro, D., Perez-Riverol, Y., Reisinger, F., Rios, D., Wang, R. & Hermjakob, H. (2013). The PRoteomics IDEntifications (PRIDE) database and associated tools: status in 2013. Nucleic Acids Res. **41**, D1063-1069. https://doi.org/10.1093/nar/gks1262.

## Figures with Legends



**Figure 1.** Complete interactome of sperm HPM developed by Cytoscape v3.8.2 of annotated proteins (n=4,273) out of total proteins (22,117) in population of 16 Holstein Friesian bulls. This demonstrates the clustering and complexity of the identified proteins. Elliptical dots in red and green represent proteins differing in intensity by at least 2-fold between the three bulls with the highest fertility index and the three bulls with the lowest fertility index (red=up-regulated; green=down-regulated).

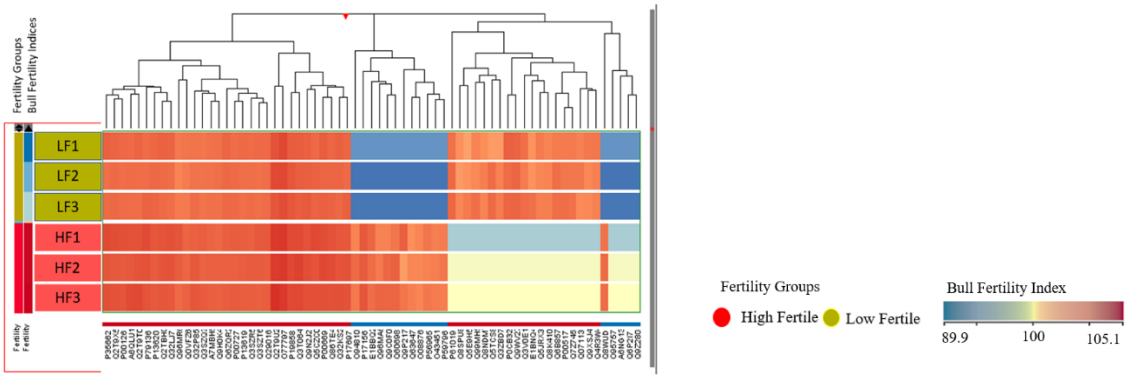


**Figure 2**. Heat map showing meta-analysis of the HPM DAPs differing by ≥ 2-fold in spectral count between high- versus low-fertility groups (HF, LF; n=3 per group) and their Bull Fertility Indices. The two vertical bars at the extreme left show Fertility Group (high, low), and Bull Fertility Indices (a scale of BFI is provided at bottom right below the heat map). Boxes between the vertical fertility bars and the heat map identify the individual bull (LF 1,2,3; HF 1,2,3) color-matched to Fertility Group (green LF, red HF). Heat map rows show individual bulls and heat map columns indicate protein accession numbers.

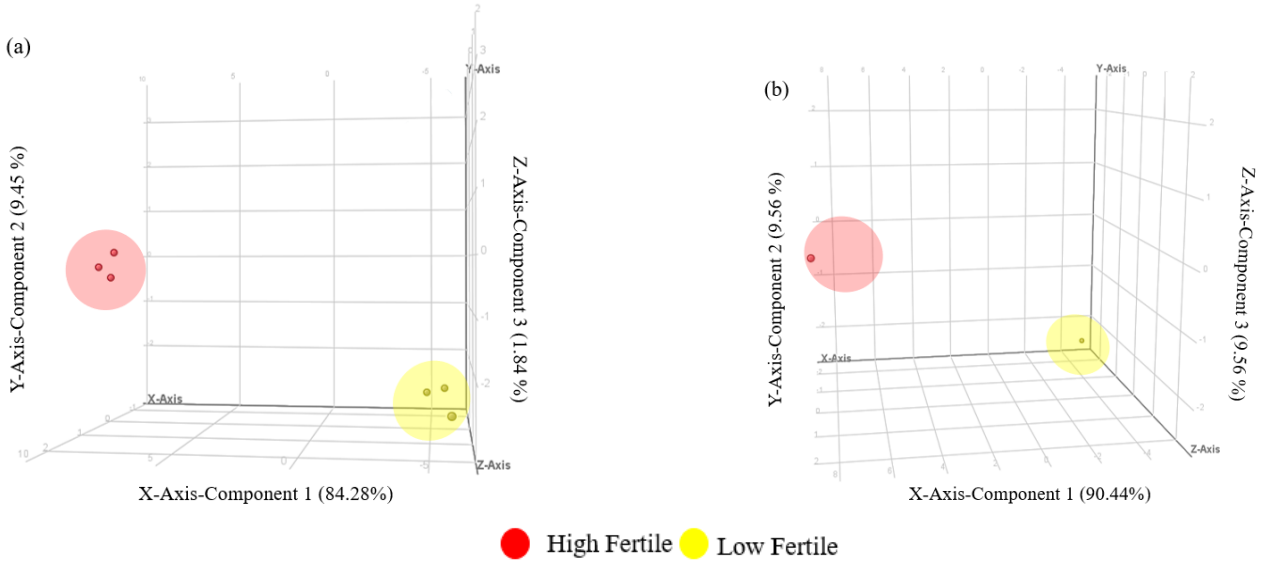


**Figure 3**. PCA plots of 67 DAPs in HPM of bull sperm of low and high fertility (n=3 per group). (a) Three-dimensional hard cluster of 67 proteins ($p < 0.05$; FC ≥ 2) (b) average of DAPs. Red dots: High Fertile; yellow dots: Low Fertile; dot size: DAPs intensity. Red circle= High fertile cluster, yellow circle= Low fertile cluster.

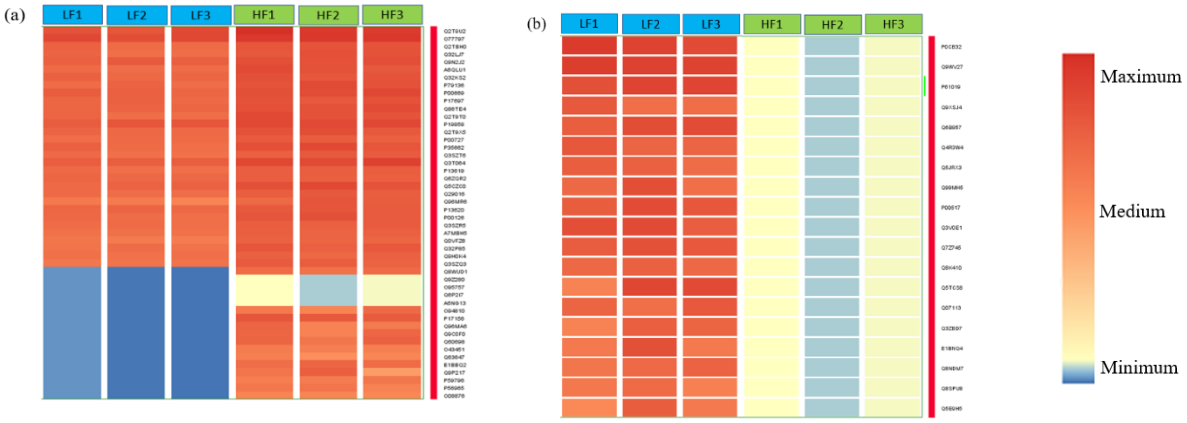


**Figure 4**. Heat map of DAPs ($p < 0.05$; FC ≥ 2) in sperm HPM of Holstein Friesian bulls of LF, and HF (n=3 per group). (a) up-regulated DAPs in sperm HPM of HF bulls. (b) down-regulated FC proteins in sperm HPM of HF bulls. Each row indicates accession numbers of every DAPs while every column shows individual bull. LF= low fertile and HF= high fertile bulls, respectively. A legend for color scale based on DAPs intensity is shown to the right of heat map.

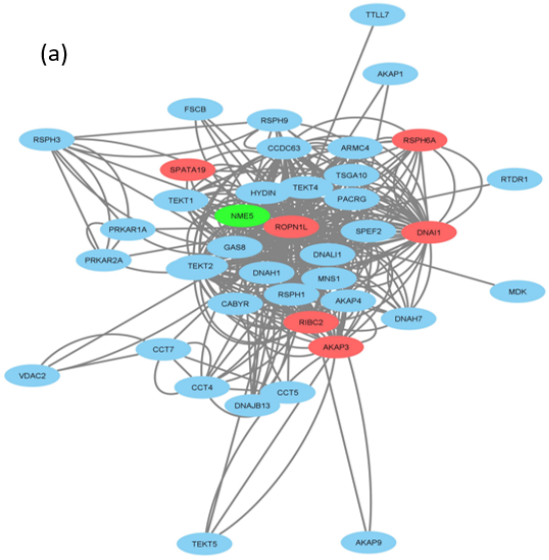


Ropporin-1-like protein

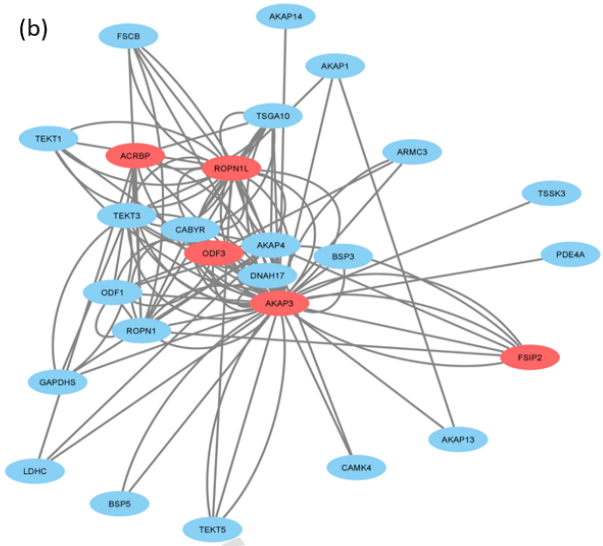


A-kinase anchor protein 3

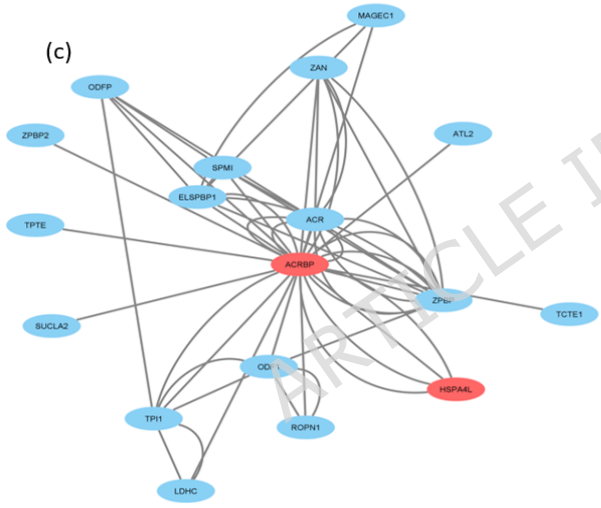


Acrosin-binding protein

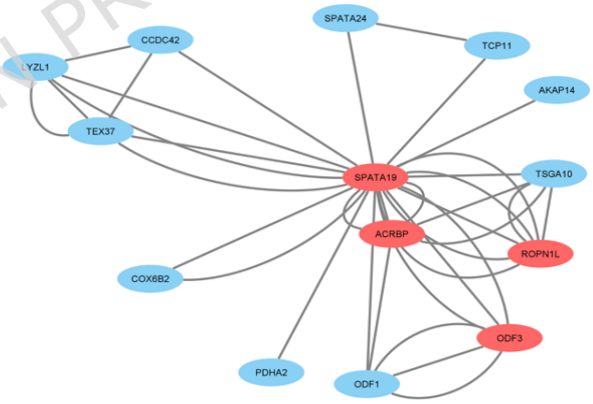


Spermatogenesis-associated protein 19

(e)

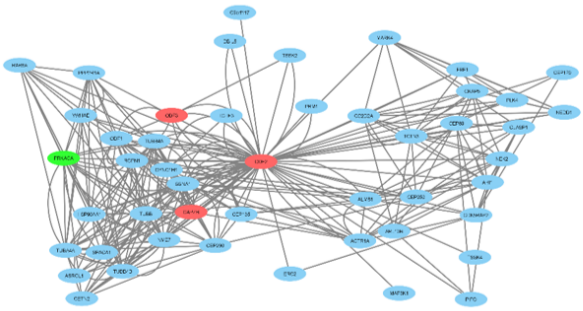

Outer dense fiber protein 2

(f)

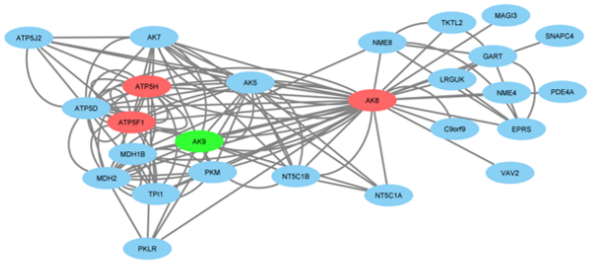


Adenylate kinase 8

(g)

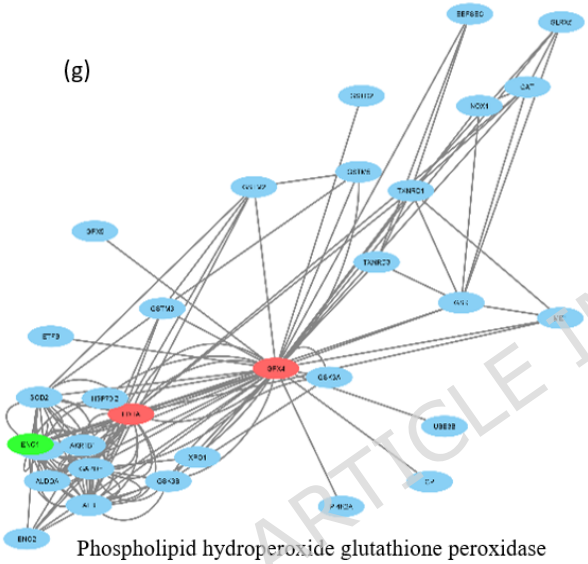

Phospholipid hydroperoxide glutathione peroxidase

(h)

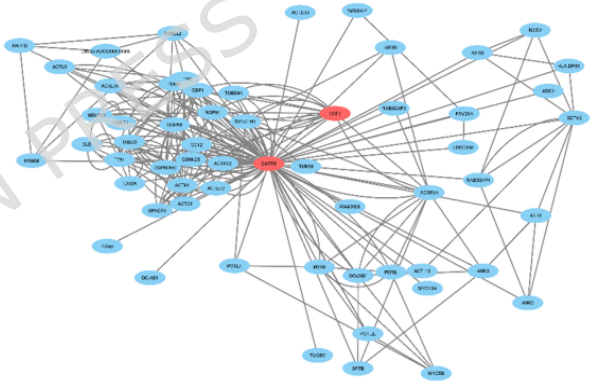

F-actin-capping protein subunit beta

(i)

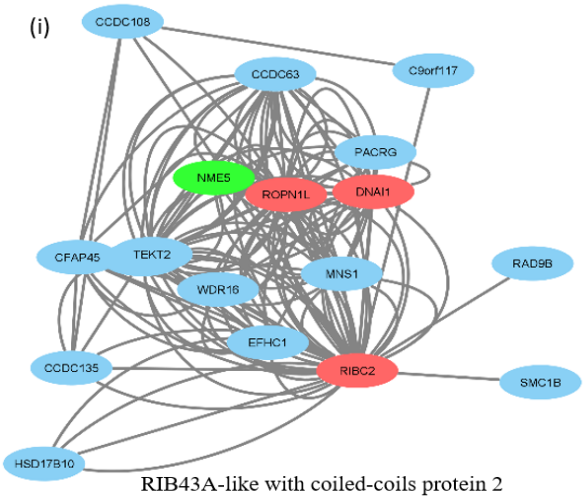


RIB43A-like with coiled-coils protein 2

(j)

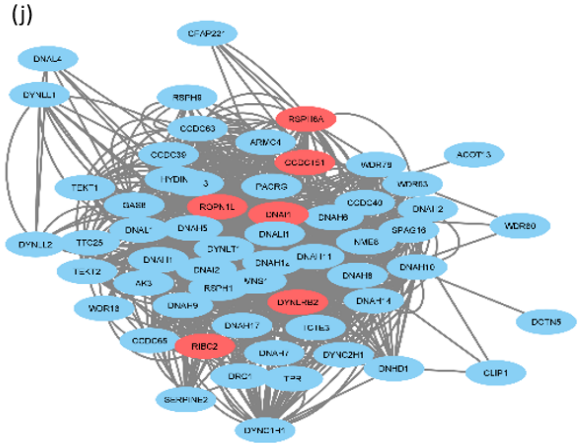


Dynein intermediate chain 1, axonemal

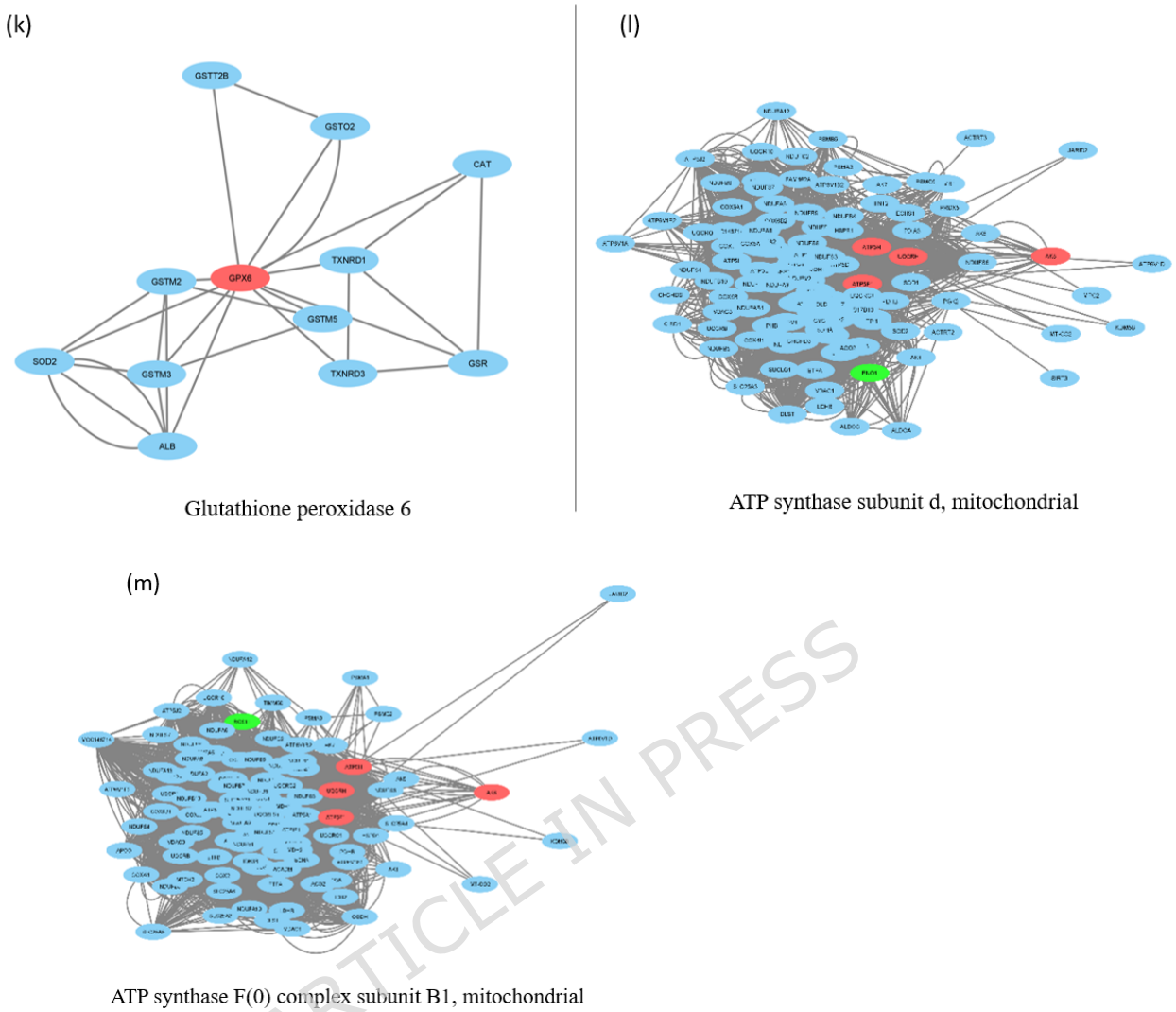




**Figure 5.** Sub-networks of selected up-regulated DAPs ($p < 0.05$; FC ≥ 2) proteins along with their IPPs (neighbor proteins in the interactome) showing different protein-protein interactions in each cluster. Ovals in red and green represent proteins differing in intensity by at least 2-fold between the three bulls with the highest fertility index and the three bulls with the lowest fertility index (red=up-regulated; green=down-regulated; blue=non-DAPs). DAPs in (a) were: Spermatogenesis-associated protein 19, Ropporin-1-like protein, RIB43A domain with coiled-coils 2, A-kinase anchor protein 3, Dynein intermediate chain 1, axonemal, Radial spoke head 6 homolog A in up-regulated and Nucleoside diphosphate kinase homolog 5 in down-regulated DAPs; (b) Acrosin-binding protein, Outer dense fiber protein 3, A-kinase anchor protein 3, Ropporin-1-like protein, Fibrous sheath interacting protein 2; (c) up-regulated DAPs: Acrosin-binding protein, Heat shock 70 kDa protein 4L; (d) up-regulated DAPs: Spermatogenesis-associated protein 19, Acrosin-binding protein, Ropporin-1-like protein, Outer dense fiber protein 3; (e) up-regulated DAPs: Outer dense fiber protein 3, Outer dense fiber protein 2, F-actin-capping protein subunit beta, down-regulated DAPs: cAMP-dependent protein kinase catalytic subunit alpha; (f) up-regulated DAPs: Adenylate kinase 8; ATP synthase F(0) complex subunit B1, mitochondrial, ATP synthase subunit d, mitochondrial; down-regulated DAPs:

Adenylate kinase 9; (g) up-regulated DAPs: Phospholipid hydroperoxide glutathione peroxidase, mitochondrial; Lactate dehydrogenase A, down-regulated DAPs: Alpha-enolase; (h) up-regulated DAPs: F-actin-capping protein subunit beta; Outer dense fiber protein 2; (i) up-regulated DAPs: RIB43A domain with coiled-coils 2, Ropporin-1-like protein, Dynein intermediate chain 1, axonemal, down-regulated DAPs; Nucleoside diphosphate kinase homolog 5; (j) up-regulated DAPs: Dynein intermediate chain 1, axonemal, Ropporin-1-like protein, RIB43A domain with coiled-coils 2, Dynein light chain roadblock-type 2, Coiled-coil domain-containing protein 151, Radial spoke head 6 homolog A; (k) up-regulated DAPs: Glutathione peroxidase 6; (l) up-regulated DAPs: ATP synthase subunit d, mitochondrial, ATP synthase F(0) complex subunit B1, mitochondrial, Cytochrome b-c1 complex subunit 6, mitochondrial, Adenylate kinase 8; (m) Cytochrome b-c1 complex subunit 6, Adenylate kinase 8, ATP synthase F(0) complex subunit B1, mitochondrial, ATP synthase subunit d, mitochondrial and down-regulated DAPs: Mitochondrial chaperone BCS1.

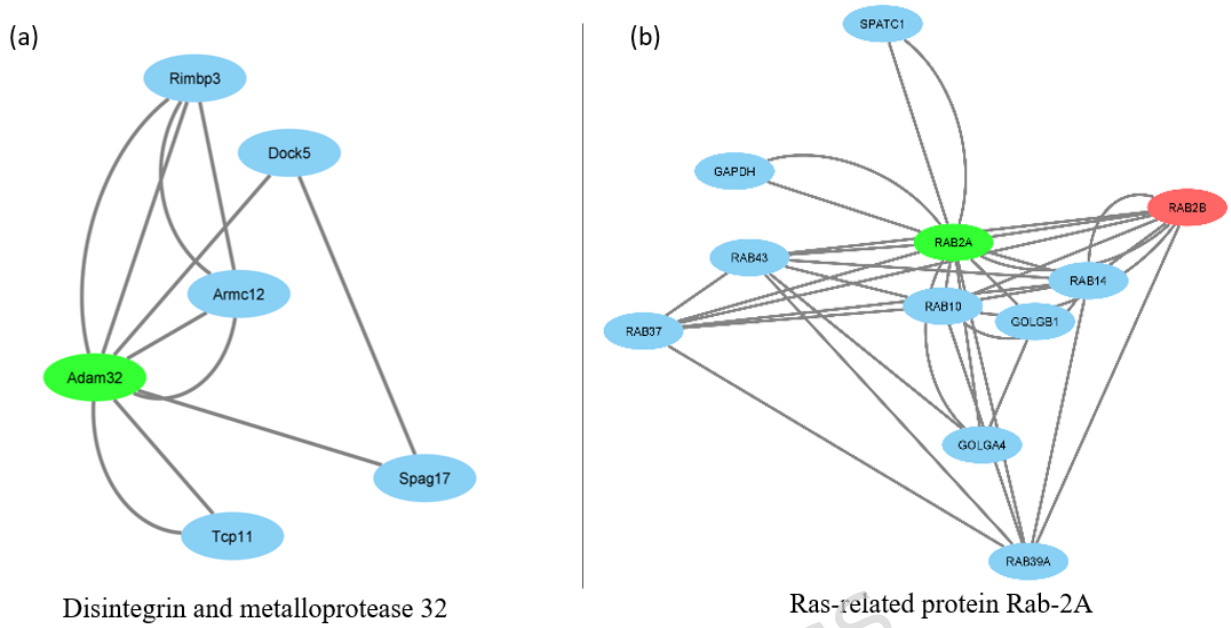


**Figure 6.** Sub-networks of selected down-regulated DAPs along with their IPPs (neighbor proteins in the interactome) showing different PPI in each cluster. Ovals in red and green represent proteins differing in intensity by at least 2-fold between the three bulls with the highest fertility index and the three bulls with the lowest fertility index (red=up-regulated; green=down-regulated; blue=non-DAPs). (a) down-regulated DAP: Disintegrin and metalloproteinase domain-containing protein 32; (b) up-regulated DAP: Ras-related protein Rab-2B, down-regulated DAP: Ras-related protein Rab-2A.

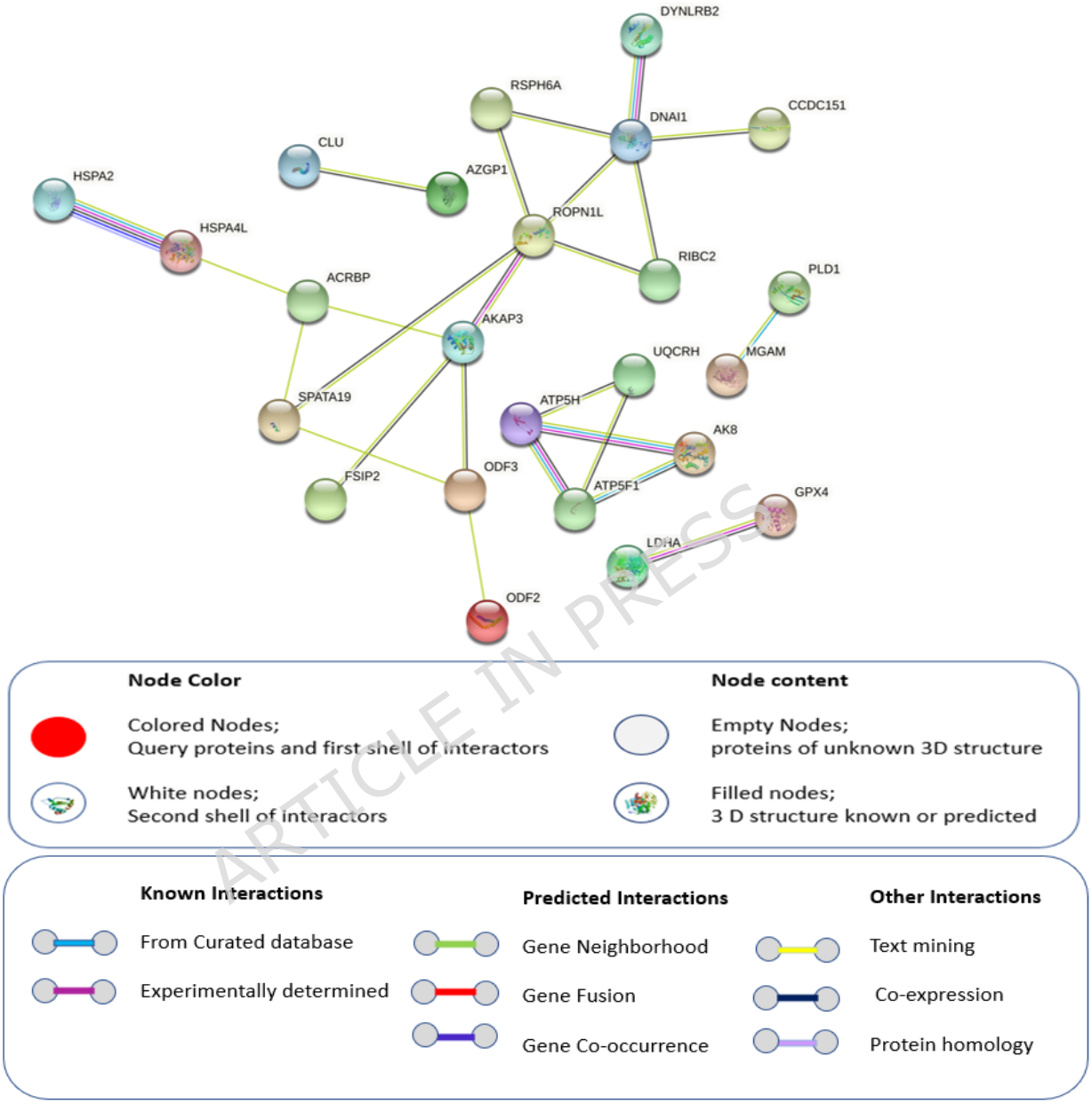


**Figure 7.** Visual mapping of up-regulated DAPs in HF sperm HPM, visualized onto a composite network based on predicted PPI network created using STRING v11.0 software together with a 'Homo sapiens' database. Each protein is symbolized as a node and associations as edges in different interactions between proteins (see legend for detail), based on the actions view of STRING v11.0. Thickness of the edges is based on confidence score.

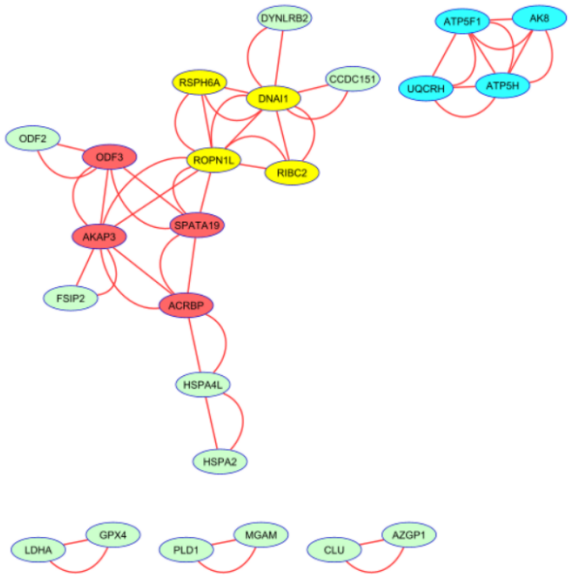


**Figure 8.** The hub protein network developed by MCODE (tool in Cytoscape v3.8.2). Three clusters exist, based on densely connected regions in the STRING network of the up-regulated DAPs. Blue ovals show hub proteins in cluster 1 having 4 nodes and 10 edges; yellow ovals show hub proteins in cluster 2 with red ovals (hub proteins in cluster 3) having 4 nodes and 8 edges; green ovals are IPPs connected to the hub proteins. The three small clusters of green ovals at the bottom are up-regulated DAPs not interacting with hub proteins.

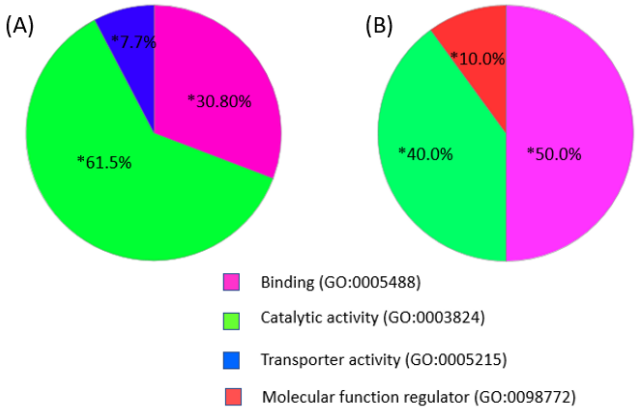


**Figure 9.** Classified sperm HPM proteins that differ by ≥ 2-fold (DAPs) between bulls with high and low fertility (HF vs LF; n= 3 bulls per group), analyzed for Molecular Functions with PANTHER database. (A) DAPs down-regulated in HF vs LF; (B) DAPs up-regulated in HF vs LF. *Molecular functions significantly different between groups.

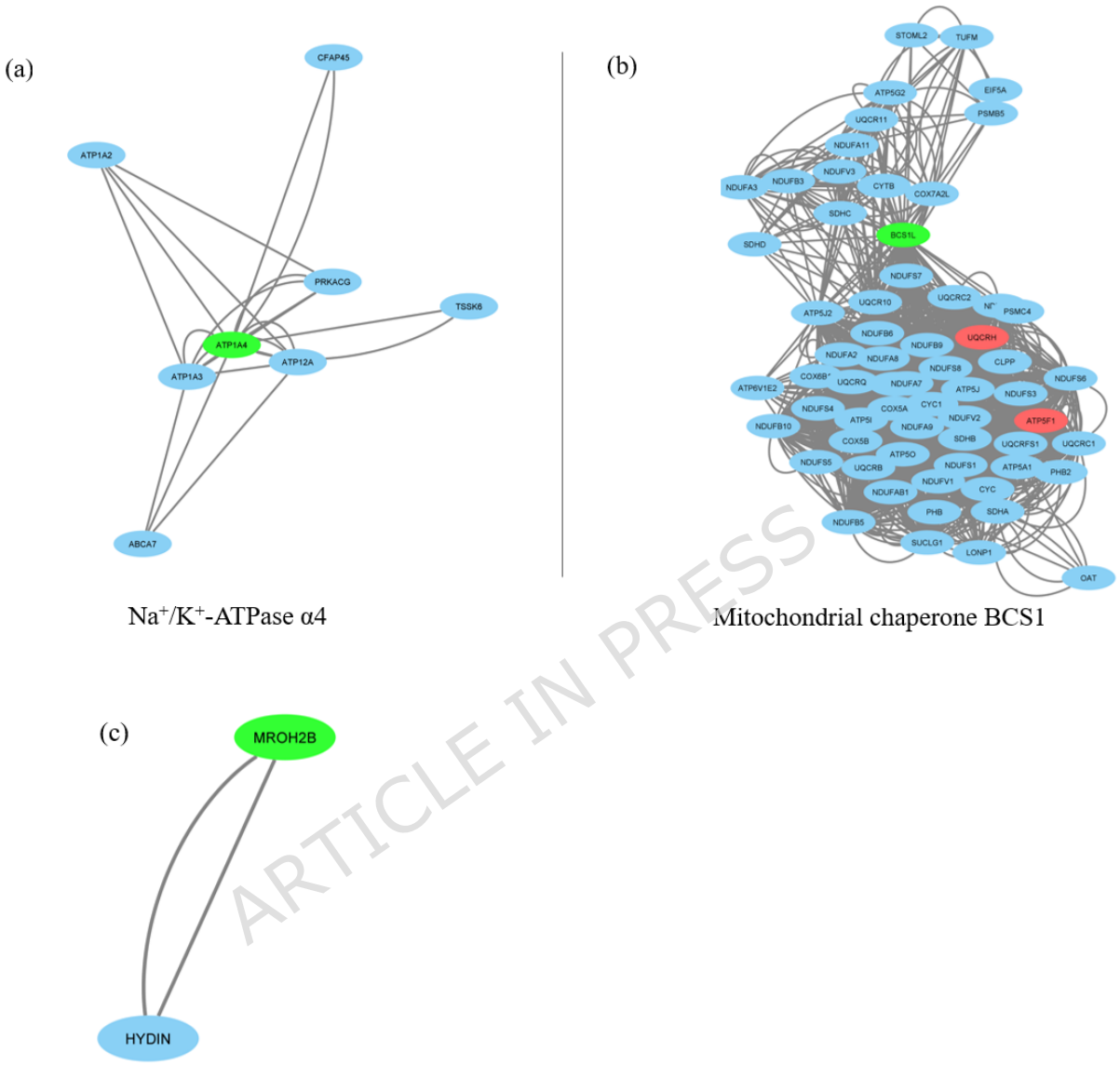


**Figure 10.** Sub-networks of selected down-regulated DAPs along with their IPPs (neighbor proteins in the interactome) showing different PPI in each cluster (n = 16). Ovals in red and green represent proteins differing in intensity by at least 2-fold between ATH (n = 8) and ATL (n = 8) bulls (red = up-regulated; green = down-regulated; blue = non-DAPs).